JACS
JOURNAL OF THE AMERICAN CHEMICAL SOCIETY
pubs.acs.org/JACS
Article

Structure and pH Dependence of Membranolytic Mechanisms by Truncated Oxidized Phospholipids

Min Xie, Maik G. N. Derks, Eveline H. W. Koch, C. Bjorn van Boven, Minchakarn Janlad, Behnaz Bagheri, Zexi Xu, Daria Kovryzhenko, Cornelis A. van Walree, Ana Sobota, Markus Weingarth, Jirasak Wong-ekkabut, Mikko Karttunen, Eefjan Breukink, J. Antoinette Killian, Andreas F. P. Sonnen, and Joseph H. Lorent*

Cite This: J. Am. Chem. Soc. 2025, 147, 9175−9189
Read Online

ABSTRACT: Membrane lipid oxidation is a universal process that occurs in situations of oxidative stress and is encountered in numerous physiological and pathological situations. Oxidized truncated phospholipids make up a large part of the oxidation products and alter the membrane properties in a way that can lead to cell death. However, the underlying mechanisms are not well understood nor is it clear whether environmental factors, such as pH, can modulate these effects. Using model membranes, we investigate how individual lipid aldehydes and carboxylic acids with truncated acyl chains alter the membrane structure. Our data shows that lipid aldehydes and carboxylic acids have different permeabilization efficiencies towards molecules of varying charge and size and that ΔC9 truncated lipids are usually more efficient in permeabilizing membranes than ΔC5. In terms of physical mechanisms, the ΔC9 truncated lipid carboxylic acid induces permeabilization and membrane curvature in a pH-dependent fashion. This is explained by ionization-dependent exposure of the carboxyl group to the water−bilayer interface, which increases the intrinsic molecular curvature of the oxidized lipid. Conversely, ΔC9 truncated lipid aldehydes and nonionized carboxyls do not induce curved structures but are more efficient in increasing permeability toward larger molecules. We further show that truncated lipids can escape the bilayer and accumulate at interfaces, implying that they might act on neighboring cells. This study indicates that oxidized phospholipids with truncated acyl chains disrupt membrane structure, depending on their specific molecular structure and the pH of the environment, opening a possible route for the design of lipid nanoparticles with pH-dependent drug release.

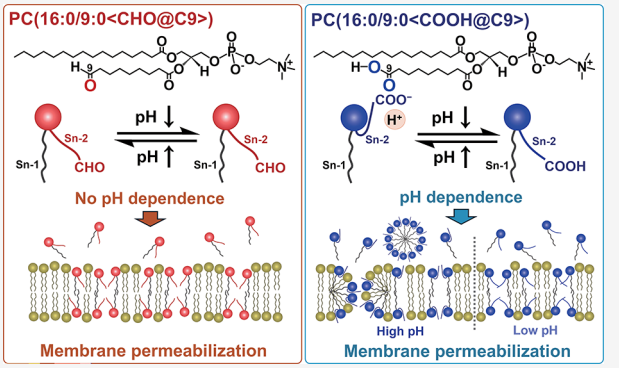

INTRODUCTION

Lipid oxidation is not only involved in various basic cellular reaction programs such as cellular senescence[1] but also contributes to pathological dysfunctions, including Parkinson's disease,[2−4] cardiovascular diseases,[5,6] diabetes,[7] and Alzheimer's disease.[8] Phospholipid bilayers are fundamental structural units of cellular membranes which are susceptible to short and long-lived reactive oxygen species (ROS).[9] The sources of ROS derive from either endogenous production, such as the mitochondrial respiratory chain in mammalian cells,[10] or exogenous stimuli, such as UV light and heat.[11,12] Generally, the majority of formed oxidation products are lipid hydroperoxides and various truncated lipid oxidation products such as aldehydes and carboxylic acids.[9,13−15] Oxidative truncation produces further smaller volatile products, such as malonyldialdehyde (MDA) and 4-hydroxynonenal (4-HNE) that derive from their parental lipids. Their electrophilic properties render these molecules very reactive towards biomolecules which supposedly leads to pathological as well as physiological processes.[16] The diversity and the physiological roles of these secondary products has been reviewed extensively.[11,17,18] While these small volatile products can diffuse passively through membrane bilayers, lipid aldehydes and lipid carboxylic acids with truncated acyl chains can alter structure and function of membrane bilayers.[19] Bilayers or lamellar phases are formed by amphipathic phospholipids that bury their hydrophobic tails in the membrane interior and expose their hydrophilic head groups to the aqueous phase.[20,21]

Lipid oxidation can disrupt the bilayer structure due to increased hydrophilicity or a radical change in lipid shape.

Received: September 10, 2024
Revised: February 18, 2025
Accepted: February 19, 2025
Published: March 5, 2025

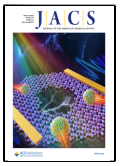

Molecular dynamics (MD) simulations show that in some cases lipid aldehydes and carboxylic acids might expose their chains with the oxidized hydrophilic functions to the membrane surface.[22−25] This change of conformation results supposedly in conically shaped lipids which increase the membrane surface area, reduce bilayer thickness,[26−28] and induce spontaneous positive curvature, which results in the formation of micelles or pores.[28,29]

The resulting defects can significantly influence the biophysical and physiological functions of the membrane bilayers. Studies show that the presence of oxidized lipids alter lipid packing differentially, depending on their structure.[9,23,28] Experimental and MD simulations have demonstrated that especially lipid aldehydes increase the membrane permeability. Free energy profile analyses indicate that the activation free energy requirement for diffusion of small hydrophilic molecules, such as H_2O, H_2O_2, and O_2, across the bilayer is much lower when lipid aldehydes are present.[28,30] Studies have further shown that lipid oxidation leads to the formation of pores in model membranes either by artificially oxidizing membranes of unsaturated lipids[9,27,31] or by incorporating certain oxidized lipids.[32,33]

Although impairment of the membrane bilayer structure induced by oxidized lipids has been reported in many studies, a systematic characterization of the permeabilization mechanisms upon structural differences of truncated oxidized lipids is still lacking and there is a need for experimental data that could confirm the conclusions that have been obtained from MD simulations.[22−25] In addition, there is almost no data on possible additive effects of different OxPCs, nor the influence of pH. A pH dependent effect could arise from ionization of the COOH group of carboxylated lipids and has been proposed in MD simulations.[34] We therefore characterized the membranolytic mechanisms by complementary techniques using model membranes of different truncated carboxylic acids and aldehydes (structures in Figure 1) upon different pHs and we investigated the additivity of these effects. We studied permeabilization towards different types of molecules in giant unilamellar vesicles (GUVs) and large unilamellar vesicles (LUVs). We further investigated lipid packing by polarity sensitive probes, induction of curvature and order parameter by ^{31}P-NMR, and the formation of micelles and the release of oxidized lipids from the membrane by dynamic light scattering and surface tension measurements. We measured the zeta (ζ)-potential to determine exposure of the ionized carboxyl group to the membrane interface and used MD simulations to explain some of the observed results and to help attribute permeabilization mechanisms to the different OxPCs.

RESULTS

Truncated Aldehydes Produce Stronger Influx of 4 kDa FITC-Dextran and Sulforhodamine B than Carboxyls. We first used GUVs to evaluate permeabilization induced by lipid aldehydes and carboxylic acids with truncated acyl chains. We observed that 20 mol% of PC(16:0/9:0<CHO@C9>) or PC(16:0/9:0<COOH@C9>) induced permeabilization toward FITC-Dextran (4 kDa) in GUVs made of PC(16:0/18:1), with a larger effect induced by PC(16:0/9:0<CHO@C9>) (Figure 2A,B). This result is further supported by a sulforhodamine B (SRB) leakage assay in GUVs containing 10 mol% of PC(16:0/9:0<CHO@C9>) or PC(16:0/9:0<COOH@C9>) (Figure S2). We observed a larger release of SRB in GUVs containing the aldehyde truncated form.

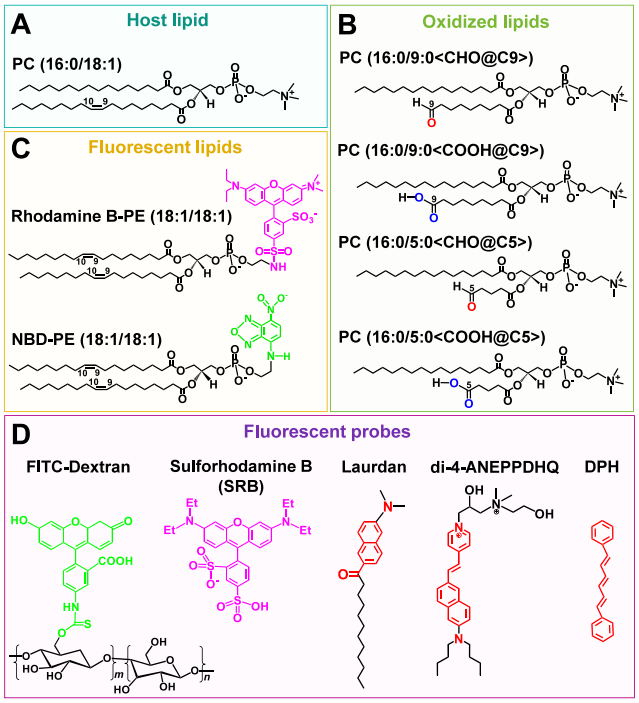

Figure 1. Chemical structures of lipids and fluorescent probes used in this study. (A) Host lipid for LUV or GUV. (B) Oxidized lipids. (C) Fluorescent lipids. (D) Fluorescent probes.

Dithionite Quenching of Inner Leaflet NBD-PE Occurs Only above a Threshold of Truncated OxPCs but the Effect Is Additive. To quantify the permeabilization and/or possibly lipid flip-flop induced by oxidized lipids in membrane bilayers, we used a dithionite quenching assay in LUVs (Figure 2C). OxPCs were integrated into PC(16:0/18:1) LUV containing headgroup labeled NBD-PE(18:1/18:1) at 0.5 % (mol/mol) and dithionite was further used to chemically quench the fluorescence of NBD irreversibly. This results in 50 % quenching if dithionite does not diffuse to the luminal monolayer of the LUV, and if there is no flopping of NBD-PE to the outside monolayer. Our results show that only around 40−45 % of quenching was attained in the controls (Figure S1). This is because of some remaining MLVs in the sample (~4 %; see Figure S3). Since the same ratio of MLVs was present throughout all conditions, we concluded that the observed effects did not result from a change of lamellarity. Triton X-100 was used to solubilize the membranes, leading to complete fluorescence quenching. To quantify the quenching by dithionite ions, we fitted the quenching curves to an exponential plateau model. The equation of this model is % quenching = $Y_M - (Y_M - Y_0)^{-kt}$, with k reflecting the rate constant (min^{-1}). Y_M and Y_0 indicate the maximum and minimum percentages of quenching, respectively. As expected, the quenching rate increased upon higher incorporated fractions of ΔC9 and ΔC5 OxPCs in LUVs, with carboxylated acyl chains being slightly more efficient in promoting quenching of NBD-PE than lipid aldehydes (Figure 2D,E, and Figure S1A,B,C,D). Interestingly, a significant increase of quenching was only observed when truncated OxPCs were present above a threshold of ~12−15 mol% (Figure 2D,E and Figure S1A,B,C,D). However, when both PC(16:0/9:0<CHO@C9>) and PC-(16:0/9:0<COOH@C9>) were mixed at different ratios but at a constant total molar fraction of 20 mol% of total oxidized lipids,

https://doi.org/10.1021/jacs.4c12543
J. Am. Chem. Soc. 2025, 147, 9175−9189

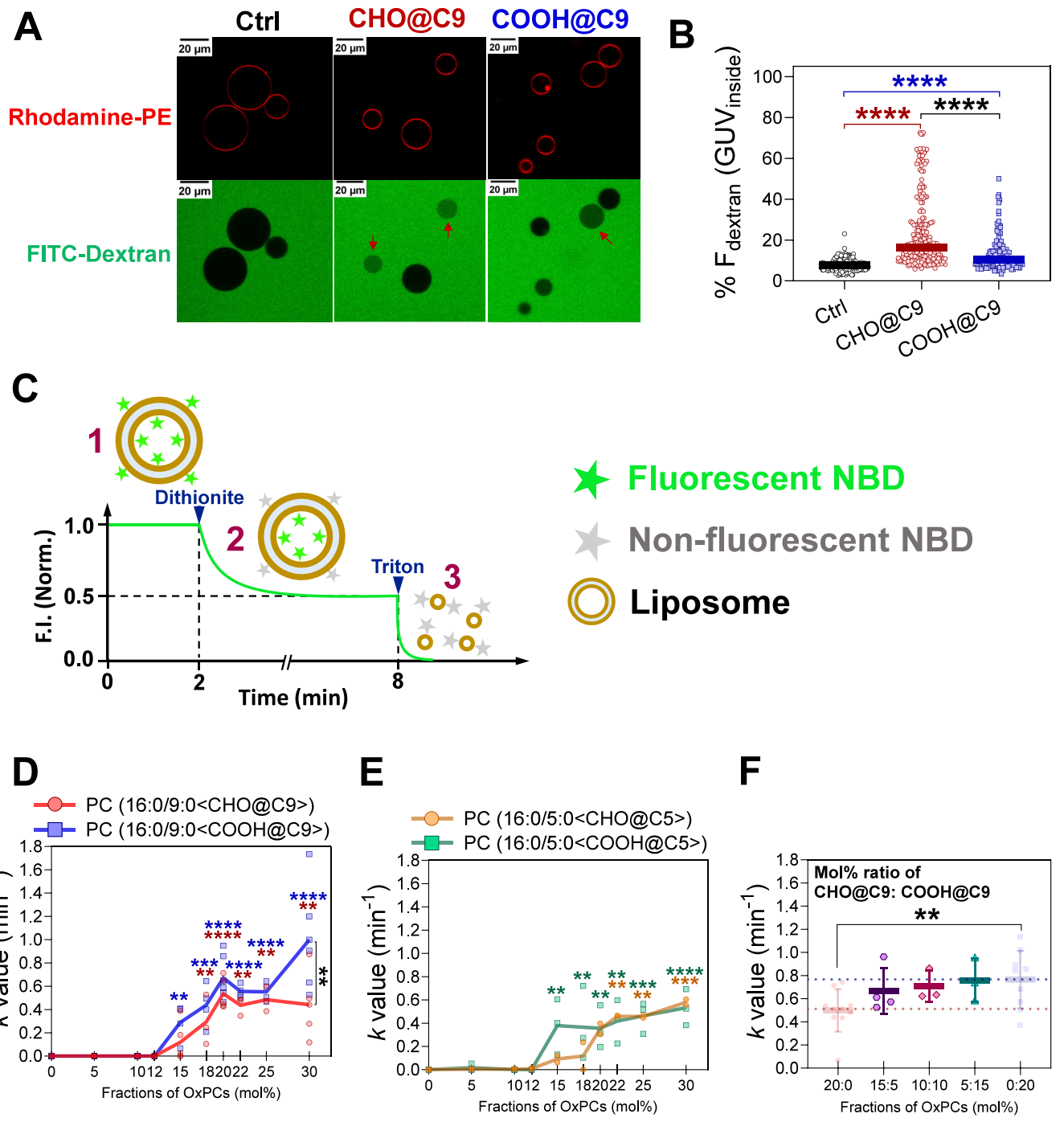

Figure 2. Incorporation of OxPCs disrupts PC(16:0/18:1) membranes. (A) Confocal microscopy images of GUVs containing no oxidized lipids (control) or 20 mol% PC(16:0/9:0<CHO@C9>) or PC(16:0/9:0<COOH@C9>) incubated for 10 min in the presence of 40 μM of FITC-Dextran (4 kDa). Red arrows indicate GUVs that are permeabilized. (B) Quantification of the FITC-Dextran intensity inside versus outside of GUVs. (C) Schematic diagram of the dithionite quenching assay. Quenching speed (k values, min^{-1}) induced by (D) ΔC9 and (E) ΔC5 truncated OxPCs and (F) varied ratios of ΔC9 truncated OxPCs at a total fraction of 20 mol% based on curve fitting with an exponential plateau model as described in Materials and Methods in the SI. One-way ANOVA analysis was used to compare fluorescence intensity in GUVs toward controls. Two-way ANOVA analysis was used to compare the k values between different incorporation fractions and the negative controls (colored stars) and the k values between PC(16:0/9:0<CHO@C9>) and PC(16:0/9:0<COOH@C9>) at the same incorporation fractions (black stars). At least two independent experiments were performed for the NBD-PE fluorescence quenching assay in triplicates ($n \geq 2$, $^{*}p < 0.05$, $^{**}p < 0.01$, $^{***}p < 0.001$, $^{****}p < 0.0001$).

quenching slightly increased with higher PC(16:0/9:0<COOH@C9>) ratios (Figure 2F and Figure S1E). Curiously, even when one of both lipids dropped below the 12−15 mol% hurdle, quenching was still observed, meaning that the observed threshold for one OxPCs is not valid if two different OxPCs are present and that somehow the effect is additive (Figure 2F and Figure S1E).

Truncated Aldehydes Induce Quicker Permeation towards Sulforhodamine B (SRB) than Carboxyls while a Low pH Enhances the Effect of Carboxyls. In addition to the dithionite assay, we examined permeabilization by adding

https://doi.org/10.1021/jacs.4c12543
J. Am. Chem. Soc. 2025, 147, 9175−9189

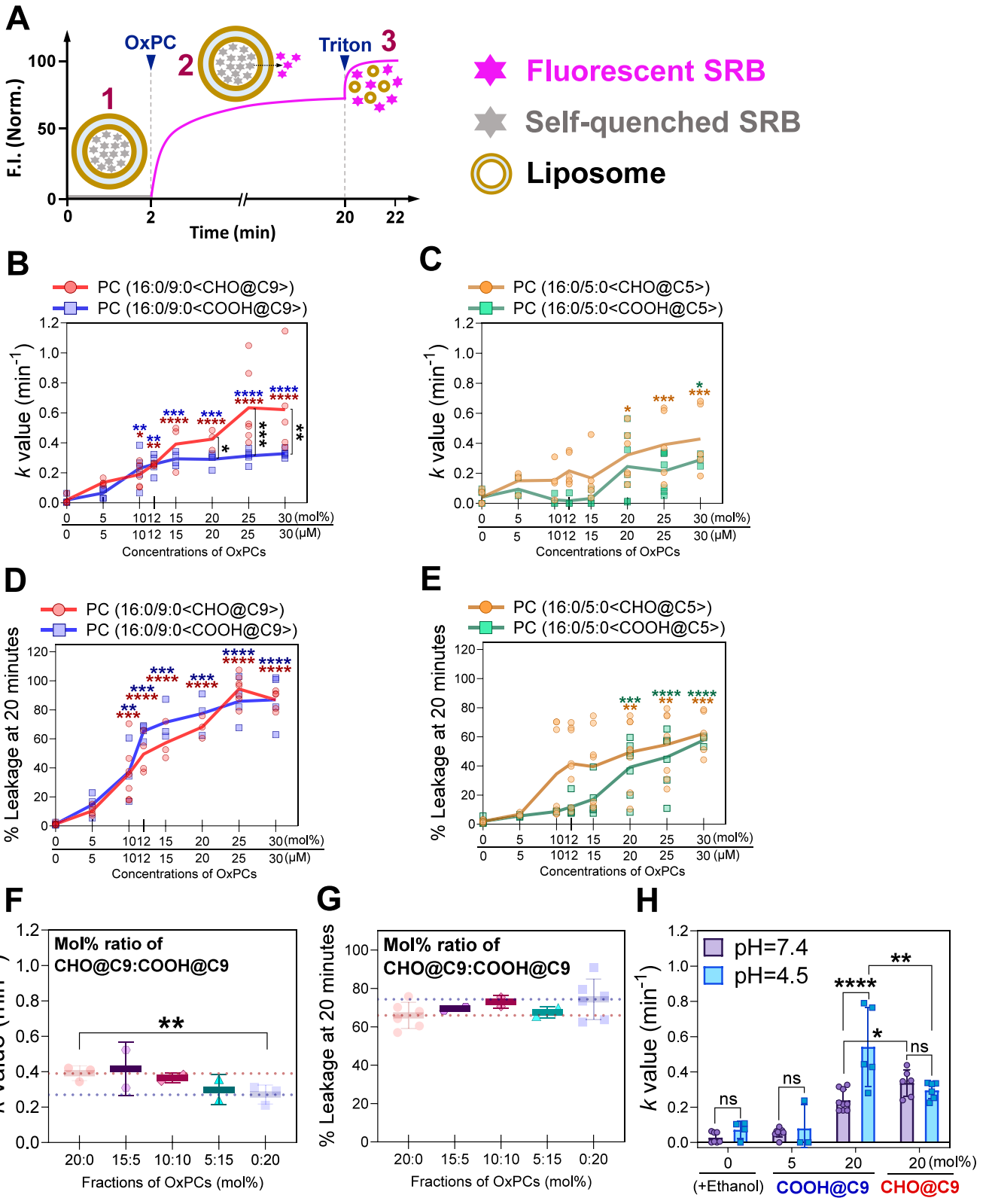

Figure 3. Permeabilization of PC(16:0/18:1) LUV induced by the addition of PC(16:0/9:0<CHO@C9>) and PC(16:0/9:0<COOH@C9>) to the suspension. (A) Schematic diagram of permeabilization assay via sulforhodamine B leakage. Release constants (***k*** value, min^{-1}) of sulforhodamine B after addition of (B) ΔC9 and (C) ΔC5 truncated OxPCs, and (F) varied ratios of ΔC9 truncated OxPCs at 20 mol% based on curve fitting as described in materials and methods. Percentage (%) of escaped sulforhodamine B at 20 min after addition of (D) ΔC9 and (E) ΔC5 truncated OxPCs and (G) variable ratios of ΔC9 aldehydes and carboxyls at a total concentration of 20 mol%. (H) Comparison of release constants (***k*** value, min^{-1}) of sulforhodamine B between buffers at pH = 7.4 and pH = 4.5. One-way ANOVA analysis was used to compare the ***k*** values and the leakage at 20 min between different fractions of each OxPCs and the corresponding controls (colored stars). Unpaired *t*-test analysis (two-tailed) was used to compare the ***k*** values between PC(16:0/9:0<CHO@C9>) and PC(16:0/9:0<COOH@C9>) at the same concentrations or different pHs (black stars). At least three independent experiments were performed ($n \geq 3$, $^{*}p < 0.05$, $^{**}p < 0.01$, $^{***}p < 0.001$, $^{****}p < 0.0001$).

https://doi.org/10.1021/jacs.4c12543
J. Am. Chem. Soc. 2025, 147, 9175−9189

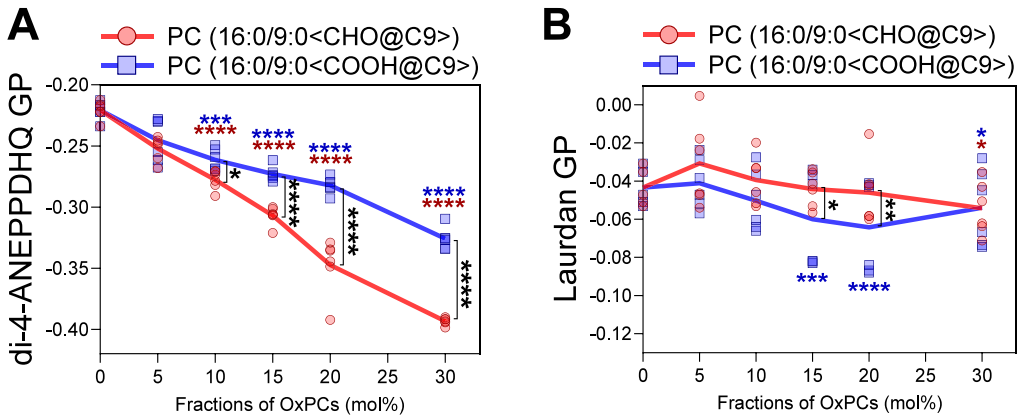

Figure 4. Membrane packing characterized by polarity sensitive probes. (A) Di-4-ANEPPDHQ GP and (B) Laurdan GP upon increasing fractions of PC(16:0/9:0<CHO@C9>) and PC(16:0/9:0<COOH@C9>) integrated into PC(16:0/18:1) LUV. Two-way ANOVA analysis was used to compare different incorporated fractions to the corresponding controls (colored stars) and between PC(16:0/9:0⟨<CHO@C9>) and PC(16:0/9:0<COOH@C9>) (black stars) at the same incorporated fractions ($n \geq 6$, *$p < 0.05$, **$p < 0.01$, ***$p < 0.001$, ****$p < 0.0001$).

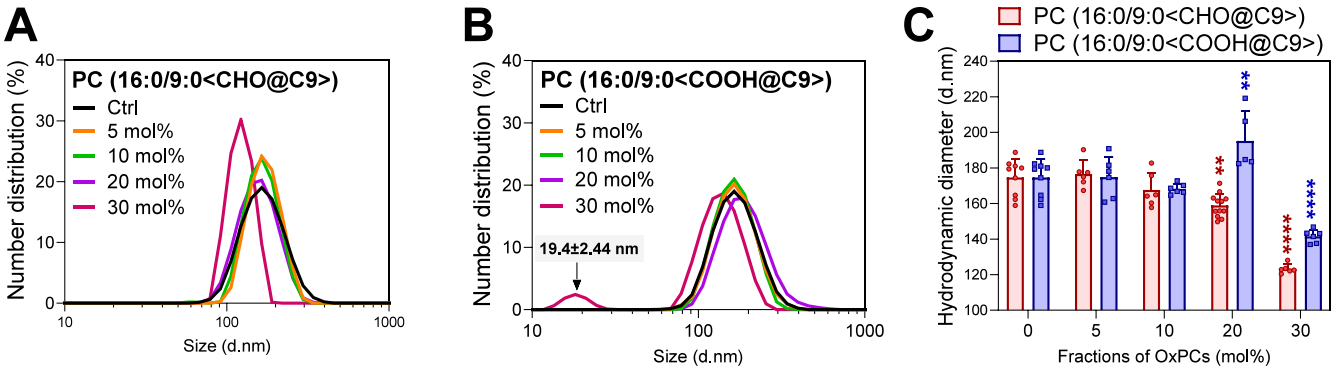

Figure 5. DLS analysis of PC(16:0/18:1) LUV containing PC(16:0/9:0<CHO@C9>) (A, C) or PC(16:0/9:0<COOH@C9>) (B, C). Size distribution of LUVs containing different amounts of (A) PC(16:0/9:0<CHO@C9>) or (B) PC(16:0/9:0<COOH@C9>). The arrow indicates the average hydrodynamic diameters in nanometers based on the second peak (smaller peak). (C) Average hydrodynamic diameters in nanometers based on the main peak (larger peak). The values are derived from 6 measurements with error bars indicating the standard deviation (SD). One-way ANOVA was used to compare the size difference between LUVs with different incorporated fractions of OxPCs toward the corresponding controls ($n \geq 6$, *$p < 0.05$, **$p < 0.01$, ***$p < 0.001$, ****$p < 0.0001$).

different OxPCs to the suspension containing PC(16:0/18:1) LUVs which enclosed sulforhodamine B at a self-quenching concentration of 20 mM (Figure 3A). Triton X-100 was used as a positive control to induce complete permeabilization. However, it induced a constant increase of SRB fluorescence that was accounted for in the calculation of release (Figure S4E). The addition of OxPCs to the suspension induced concentration-dependent permeabilization (Figure S4A,B,C,D, arrows indicate the addition of OxPCs). As controls, equal amounts of ethanol and PC(16:0/18:1) lipid were added, and neither of them induced permeabilization (Figure S4A,B,C,D). As for the quenching assay, we fitted the release curves with the exponential plateau model. The k value showed that ΔC9 and ΔC5 lipid aldehydes induced faster permeabilization than ΔC9 and ΔC5 carboxylic OxPCs, respectively (Figure 3B,C and Figure S4A,B,C,D). Curiously, the opposite was observed for dithionite quenching (Figure 2D,E). However, after 20 minutes, PC(16:0/9:0<CHO@C9>) and PC(16:0/9:0<COOH@C9>) induced a similar level of release at 91.5 % and 87.0 %, respectively (Figure 3D,E). Further, ΔC9 truncated lipids were slightly more effective in releasing SRB than ΔC5 truncated lipids (Figure 3B,C and Figure S4A,B,C,D). SRB release induced by varying ratios of PC(16:0/9:0<COOH@C9>) upon PC(16:0/9:0<CHO@C9>) at a total of 20 mol% was not significantly altered (Figure 3F,G), consolidating the hypothesis that the effect on permeability of truncated lipids with different chemical functions is additive.

To investigate the probable pH dependence of SRB release because of the protonatable carboxyl function, we also assessed SRB leakage under acidic conditions (pH = 4.5). Importantly, PC(16:0/9:0<COOH@C9>) induced a quicker permeabilization in acidic (pH = 4.5) medium, whereas no significant changes were observed with PC(16:0/9:0<CHO@C9>) upon pHs (Figure 3H and Figure S4G). This suggests that nonionized carboxyl and aldehyde functions are somehow more efficient in releasing SRB.

Truncated Lipid Aldehydes Alter Membrane Polarity and Membrane Fluidity Differently from Carboxyls. Polarity sensitive probes, such as Laurdan and di-4-ANEPPDHQ, have recently been shown to report different trends upon increasing membrane oxidation.[9] In theory, these probes should be able to sense increased water insertion or a change of polarity in their microenvironment that is quantified by the generalized polarization (GP).[35] The fluorophore of di-4-ANEPPDHQ is assumed to localize at the membrane interface and determine properties of only the outer leaflet of the

https://doi.org/10.1021/jacs.4c12543
J. Am. Chem. Soc. 2025, 147, 9175−9189

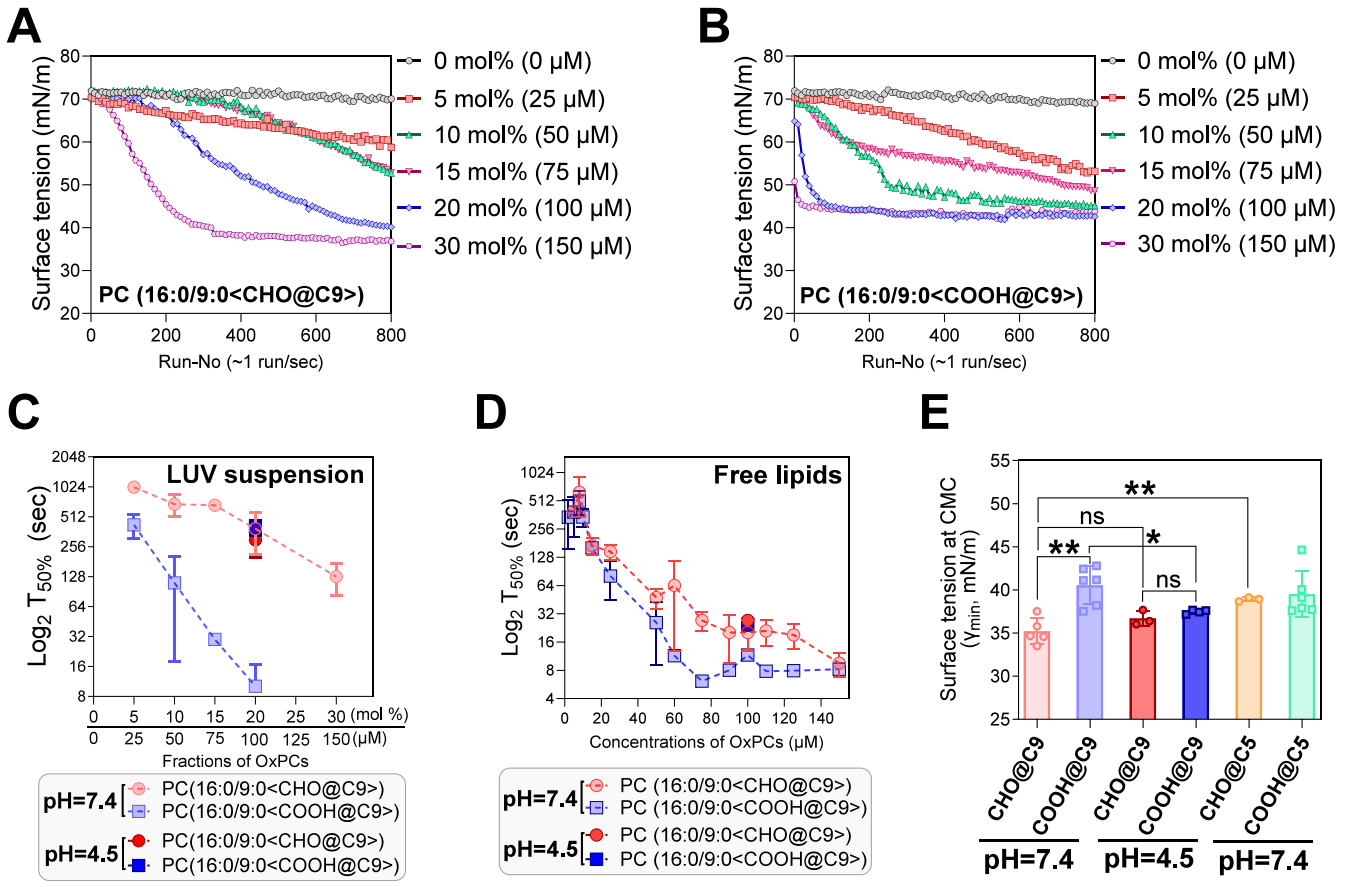

Figure 6. Surface tension determination with pendant drop tensiometry. Interfacial tension of PBS suspensions containing PC(16:0/18:1) LUVs that have been incorporated with different amounts of (A) PC(16:0/9:0<CHO@C9>) and (B) PC(16:0/9:0<COOH@C9>) upon inspection time. The $\log_2 T_{50\%}$ values of surface tension reduction in the suspension containing (C) LUVs with different amounts of OxPCs (LUVs suspension) or (D) different concentrations of free OxPCs that have been added to the buffer and that do not contain LUVs (free lipids, see also Figure. S6). The $\log_2 T_{50\%}$ values were obtained by fitting the curves with a sigmoidal model using GraphPad Prism as described in the main text. (E) Minimal surface tension (γ_{min}, mN/m) at critical micellar concentration (CMC) and beyond reached by the different oxidized lipids. At least two independent experiments were performed for surface tension measurements ($n \geq 3$). The values are the mean ± SD ($n \geq 3$). One-way ANOVA was used to compare the γ_{min} (mN/m) values between different OxPCs (*$p < 0.05$, **$p < 0.01$, **$p < 0.001$, ****$p < 0.0001$).

membrane bilayer due to its positive charge and the absence of flipping,[36,37] while Laurdan is supposedly localized in between headgroups and acyl chains and probes both leaflets of the membrane bilayer.[38] We investigated here how defined molar ratios of truncated carboxylic and aldehyde OxPCs alter the GP of these probes with the aim of investigating changes in packing or membrane water incursion (Figure 4). In addition, we measured the effect on DPH fluorescence anisotropy to determine the environmental fluidity of the lipid acyl chains (Figure S5).[39]

We first observed that the incorporation of both OxPCs decreased di-4-ANEPPDHQ GP upon their present concentrations, with PC(16:0/9:0<CHO@C9>) causing larger effects than PC(16:0/9:0<COOH@C9>) (Figure 4A). Less membrane packing alterations were observed by Laurdan GP, although PC(16:0/9:0<COOH@C9>) decreased Laurdan GP significantly at concentrations higher than 10 mol% (Figure 4B). The fluidity of the hydrophobic core, probed by DPH anisotropy, seemed to be only slightly affected by both OxPCs (Figure S5).

Taken together, we observed that carboxylated and aldehyde OxPCs affect membrane packing differently.

OxPCs Reduce the Vesicle Size but Only Carboxylated Lipids Induce the Formation of a Population of Small Aggregates. To investigate if OxPCs alter the vesicle structure in LUVs by inducing the formation of micelles or other potential amphiphilic aggregates, we measured LUV size by dynamic light scattering (DLS) upon increasing fractions of truncated OxPCs. We observed that both PC(16:0/9:0<CHO@C9>) and PC-(16:0/9:0<COOH@C9>) reduced the size of PC(16:0/18:1) LUVs in a concentration dependent manner (Figure 5A,B,C). In addition, at 30 mol% of PC(16:0/9:0<COOH@C9>), we observed the formation of small aggregates with an average hydrodynamic diameter of 19 nm (Figure 5B, arrow indicates the second peak formation). To confirm a size reduction of vesicles, we did some cryo-EM measurements at pH = 7.4 and 4.5 and obtained a reduction of vesicles size specifically with PC(16:0/9:0<COOH@C9>) at pH = 7.4 (Figure S3G).

Truncated OxPCs Are Released from the Lipid Bilayer with Different Kinetics and Effects on Surface Tension while pH Influences Strongly PC(16:0/9:0<COOH@C9>) Behavior. We recently showed that complex oxidation of lipids leads to a decrease of surface tension at the air−water interface because of the release of certain oxidized species from the membrane.[9] Since truncated lipids should have a higher water solubility and possibly form micelles because of their high intrinsic molecular curvature, we wanted to measure the capacity of these lipids to leave the lipid bilayer, which also might explain

https://doi.org/10.1021/jacs.4c12543
J. Am. Chem. Soc. 2025, 147, 9175−9189

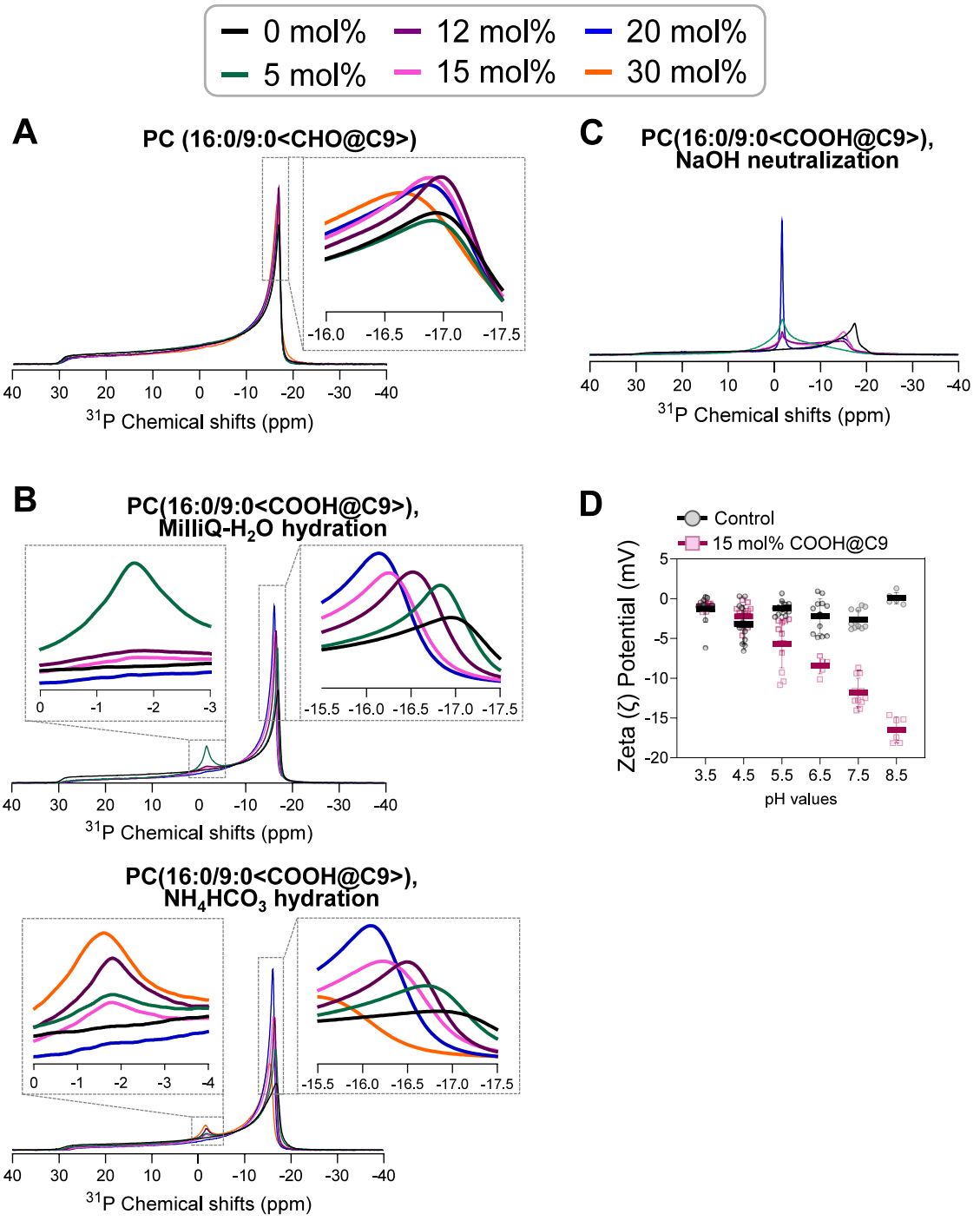

Figure 7. ^{31}P-NMR analysis and Zeta (ζ) potential determination. Static ^{31}P-NMR spectra of PC(16:0/18:1) MLVs incorporated with different fractions of (A) PC(16:0/9:0<CHO@C9>) and (B) PC(16:0/9:0<COOH@C9>) hydrated with Milli-Q-H_2O (top panel), NH_4HCO_3 (bottom panel) or (C) PC(16:0/9:0<COOH@C9>) neutralized with NaOH at an equivalent amount. (D) Zeta (ζ) potential determination in LUVs composed of PC(16:0/18:1) with or without 15 mol% of PC(16:0/9:0<COOH@C9>) upon pH changes.

the reduction of vesicle size (Figure 5). Pure PC(16:0/18:1) LUVs did not significantly affect the surface tension of the suspension within the inspected period while the incorporation of both OxPCs into LUVs reduced the surface tension of the buffer at both neutral (pH = 7.4) and acidic (pH = 4.5) pHs (Figure 6A,B and Figure S6D). This indicates that a certain amount of OxPCs left the bilayer phase of LUVs and adsorbed at the air−water interface. The rate of surface tension reduction was strongly influenced by the nature of the truncated species and the respective molar ratio inside the vesicles (Figure 6A,B).

To compare these effects to a system where no lipid bilayer was present, we measured surface tension reduction of free lipids added to the buffer (Figure S6A,B,C,E). To quantify the rate of surface tension reduction of the different concentrations of OxPCs in both data sets, we applied a four-parameter sigmoidal regression model:

$$\gamma = \gamma_{\min} + \frac{(\gamma_{\max} - \gamma_{\min})}{1 + 10^{(\log T_{50\%} - t)\times a}}$$

https://doi.org/10.1021/jacs.4c12543
J. Am. Chem. Soc. 2025, 147, 9175−9189

Here, γ is the surface tension upon time, γ_{min} is the minimal surface tension obtained (Figure 6E), γ_{max} is the initial surface tension, $T_{50\%}$ is the time in seconds necessary to reach the inflection point of the sigmoid, t is the time in seconds, and a is the slope.

We observed that free lipids added to the buffer reduced surface tension quicker than when they were incorporated into LUVs (Figure 6 and Figure S6A,B) at the same molar fractions. In addition, PC(16:0/9:0<COOH@C9>) reduced surface tension quicker than PC(16:0/9:0<CHO@C9>) (~3−5 $\log_2$), especially when OxPCs were incorporated into LUV at 20−30 mol% at pH = 7.4 (Figure 6C). This implies that PC(16:0/9:0<COOH@C9>) is easily released from the membrane bilayer either because its ionized carboxyl residue renders it more soluble in the aqueous phase and therefore can quicker migrate to the interface or because it forms more efficiently micelles or other lipid aggregates that can quickly interchange lipids with the interface. Interestingly, the time to reach the inflection point ($T_{50\%}$) drastically decreased from 403.4 s to 10.15 s for the carboxylated lipid when the pH increased from 4.5 to 7.4 (Figure 6C and Figure S6D), while the kinetics of the CHO lipid were not strongly altered (Figure 6C and Figure S6D). This indicates that the protonated carboxylated lipid remained longer in the LUVs than in the ionized version.

Based on the curve regressions made from concentrations that reached the minimum surface tension, γ_{min} (mN/m) at CMC (Figure 6E), we observed that PC(16:0/9:0<CHO@C9>) reduced surface tension to a lower value than PC(16:0/9:0<COOH@C9>) at pH = 7.4. Importantly, at pH = 4.5, the surface tension reduction of PC(16:0/9:0<COOH@C9>) became similar to that of PC(16:0/9:0<CHO@C9>) (Figure 6E). In addition, we observed that OxPCs with the same functional groups, the ones with shorter acyl chains (truncation at ΔC5), had a slightly weaker capacity to reduce surface tension (Figure 6E). In lipid monolayers, the maximum reduction of surface tension would correspond to the maximum of surface pressure obtained with a lipid at complete coverage of the water/air interface[40] or to the critical micellar concentration (CMC),[20] although the CMC might not always correspond to complete coverage of the monolayer at collapse.[41] The different capacities of reducing surface tension of both OxPCs and the pH dependence that is observed for PC(16:0/9:0<COOH@C9>) suggests different behaviors which strongly depend on the molecular structure and the pH.[42] Since the only difference between these two OxPCs is the functional group at the truncated tail, it is reasonable to assume that PC(16:0/9:0<CHO@C9>) can form more compressed monolayers than PC(16:0/9:0<COOH@C9>) at pH = 7.4, which might depend on the fact that the tail of lipid aldehydes might not protrude the same way to the interface as lipid carboxyls.[24,25] A collapse at a lower coverage or surface pressure, corresponding to a higher surface tension, might also be induced by higher solubility of the carboxyl truncated lipid or the shorter acyl chain (ΔC5) in the aqueous phase.[43] Since a low pH increases the capacity of PC(16:0/9:0<COOH@C9>) to reduce surface tension to a similar amount as PC(16:0/9:0<CHO@C9>), we can assume that both molecules adopt a similar conformation at low pH.

^{31}P-NMR Analysis Reveals a Different Effect of Truncated Carboxyls and Aldehydes on the Bilayer Structure. Membrane bilayer structure in the presence of OxPCs with truncated acyl chains was further analyzed by phosphorus NMR (^{31}P-NMR), which provides information on dynamics and structure at the phosphate group of phospholipids.[44] The static ^{31}P-NMR spectra for PC(16:0/18:1) in the presence of different fractions of PC(16:0/9:0<CHO@C9>) and PC(16:0/9:0<COOH@C9>) are displayed in Figure 7. In the presence of both OxPCs, the membranes remained mostly in a liquid crystalline lamellar phase upon increasing fractions of OxPCs (Figure 7A,B), but a small isotropic peak at lower fractions of PC(16:0/9:0<COOH@C9>) emerged (Figure 7B, top panel). Since concentrations of lipids were quite high in this MLV assay and since the protonated PC(16:0/9:0<COOH@C9>) might hence exceed the buffer capacity, we used an ammonium bicarbonate solution to increase ionization of the carboxyl function beforehand (Figure 7B, bottom panel). Under these conditions, we observed a concentration-dependent shift of the right shoulder but still not a concentration-dependent increase of the isotropic peak at ~−2 ppm, even though it was strongest at 30 mol% (Figure 7B, bottom panel).

The chemical shift anisotropy gives an indication of rotational diffusion of phospholipids and the size of the vesicles.[45] A much larger effect on chemical shift anisotropy was reached with PC(16:0/9:0<COOH@C9>) than PC(16:0/9:0<CHO@C9>) which might indicate the formation of smaller structures (increased averaging by rotational diffusion, due to a slightly different orientation) and/or a change in headgroup dynamics (Figure S7A).

In addition to the effects from individual OxPCs, we also measured the effects from the mix of PC(16:0/9:0<CHO@C9>) and PC(16:0/9:0<COOH@C9>) at a ratio of 1:1 and a total faction of 20 mol% (Figure S7C). The increased fraction of PC(16:0/9:0<COOH@C9>) led to a larger chemical shift anisotropy (Figure S7D), as expected.

Ionization of the Carboxyl Group in PC(16:0/9:0<COOH@C9>) Induces Highly Curved Structures in a pH Dependent Way. The ^{31}P-NMR results point out that the pH plays a major role in the effects induced by PC(16:0/9:0<COOH@C9>) and that the carboxyl functional group is able to significantly alter the structure of the membrane if it is ionized, possibly by producing micelles or other curved lipid aggregates. To further investigate the effect of pH on ionization of the carboxyl group and membrane structure, we used NaOH at an equivalent amount to PC(16:0/9:0<COOH@C9>) to completely ionize the carboxyl group. Under these conditions, we observed a large disruption of the lamellar structure and formation of an isotropic phase, pointing to the possibility that the intrinsic molecular curvature of the ionized PC(16:0/9:0<COOH@C9>) increases largely with pH (Figure 7C). This effect was temperature dependent (Figure S7B), with high temperatures favoring highly curved structures. To monitor the importance of pH on the ionization of PC(16:0/9:0<COOH@C9>), we measured the zeta (ζ) potential of LUVs containing PC(16:0/9:0<COOH@C9>) upon pH changes. We observed that the ζ-potential decreased strongly upon increasing pH, indicating that the ionization of the carboxyl function in the membrane depended on pH (Figure 7D). This result further suggests that the ionized carboxyl function contributes to the ζ-potential and is probably localized at the membrane−water interface.

MD Simulations Reveal Differences in Positioning and Effects on Bilayer Structure of Truncated Carboxyls and Aldehydes. To further investigate the positions of the carboxyl and aldehyde groups in the bilayer plane, we performed MD simulations (Figure 8). We observed that the ionized carboxyl

https://doi.org/10.1021/jacs.4c12543
J. Am. Chem. Soc. 2025, 147, 9175−9189

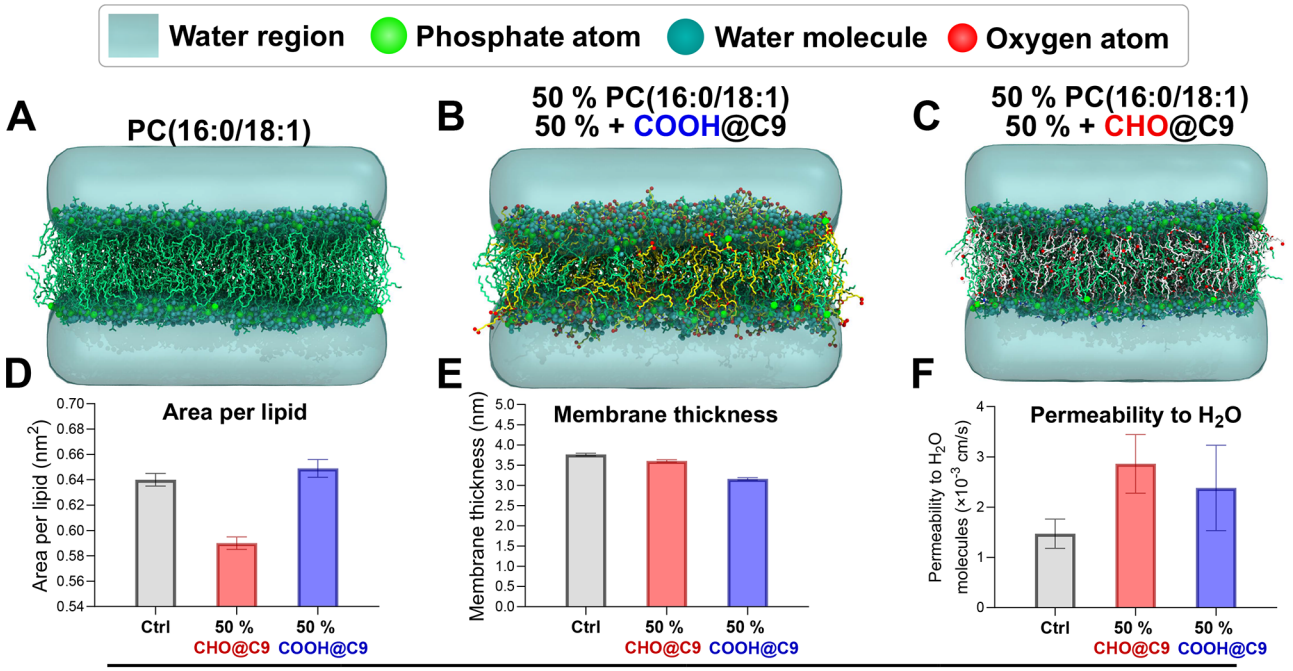

System	100 % PC(16:0/18:1)	50 % CHO@C9	50 % COOH@C9
K_A (N/m)	0.47±0.05	0.41±0.12	0.25±0.07
K_C $(\times 10^{-20} J)$	14.90±1.43	11.50±3.48	4.85±1.36

Figure 8. MD simulations of PC(16:0/18:1) membrane bilayer in the presence of OxPCs. Snapshots at the end of the 1 μs simulation of (A) 100 mol% concentration of PC(16:0/18:1), at the end of the 2 μs simulations of (B) 50 mol% PC(16:0/9:0<COOH@C9>), ionized and deprotonated, and (C) 50 mol% PC(16:0/9:0<CHO@C9>). The light blue region is water. The cyan spheres are water molecules within 3.5 Å of the phosphate atom of PC(16:0/18:1) and oxidized lipids. The green spheres are phosphate atoms of the lipid headgroups, and the green, yellow, and white lines represent PC(16:0/18:1), PC(16:0/9:0<COOH@C9>), and PC(16:0/9:0<CHO@C9>) molecules, respectively. Calculations of (D) area of per lipid, (E) thickness, and (F) permeability to water molecules in the presence of 50 mol% PC(16:0/9:0<CHO@C9>) and PC(16:0/9:0<COOH@C9>), respectively. The table shows the area compressibility modulus (K_A) and bending modulus (K_c) in the presence of OxPCs.

group pointed to the bilayer interface (Figure 8B), while the aldehyde function remained in the hydrophobic core (Figure 8C). This resulted in a slightly larger area/molecule for the truncated carboxylic acid, while the aldehyde function effectively reduced this parameter (Figure 8D). The reduction of the area per lipid by the lipid aldehyde could be in line with the reduction of surface tension that was more efficient with the aldehyde lipid. A smaller molecular volume of the CHO molecule would mean a higher density of molecules at the water−air interface and hence a lower surface tension.

Thickness was more reduced with the ionized COOH lipid (Figure 8E), meaning it can probably more efficiently abolish the bilayer structure, as observed in NMR studies (Figure 7). In terms of water permeability, we observed a slightly higher value for the CHO truncated lipid (Figure 8F). This could be in line with the permeability observed toward SRB (Figure 3 and Figure S2).

The mechanical properties of the bilayer (i.e., the area compressibility modulus (K_A) and the bending modulus (K_c)), as from of our MD trajectories, were strongly reduced by PC(16:0/9:0<COOH@C9>), while PC(16:0/9:0<CHO@C9>) had only little effects (table in Figure 8). These values reinforce the current picture that PC(16:0/9:0<COOH@C9>) has a stronger tendency to impair the bilayer structure of the membrane.

DISCUSSION

Our results show that truncated oxidized lipids have different mechanisms to destabilize lipid membranes. Permeabilization depends on the position of the acyl chain break, with ΔC9 lipids being more effective in permeabilizing membranes than ΔC5, and on the functional group at the truncation site (carboxyl or aldehyde). For truncated lipids with carboxyl groups, the pH largely influences ionization of the carboxyl group, and ionization at high pH promotes the disruption of the bilayer structure, release of carboxylated lipids from the bilayer, and formation of highly curved isotropic lipid aggregates while sulforhodamine B and FITC-Dextran leakage is higher for non-ionized residues.

Permeabilization driven by oxidized lipid aldehydes and carboxylic acids has been investigated by many groups but no clear permeabilization mechanisms have been established.[28,32,47,48] Our data suggest different permeabilization mechanisms for truncated oxidized lipids containing aldehyde and carboxyl termini and pH dependence of the mechanism for carboxyls. Lipid aldehydes were more efficient in increasing permeability toward larger molecules, including sulforhodamine B (Figure 3, Figure S2) and FITC-Dextran (Figure 2A,B), which has a hydrodynamic radius above 1 nm.[49] Non-ionized carboxyl at ΔC9 was also more efficient in releasing SRB than its ionized version (Figure 3H).

Ionized lipid carboxylic acids seemed to be more efficient in inducing permeabilization toward dithionite ions or increasing lipid flip-flop of NBD-PE than aldehydes (Figure 2D,E,F).

https://doi.org/10.1021/jacs.4c12543
J. Am. Chem. Soc. 2025, 147, 9175−9189

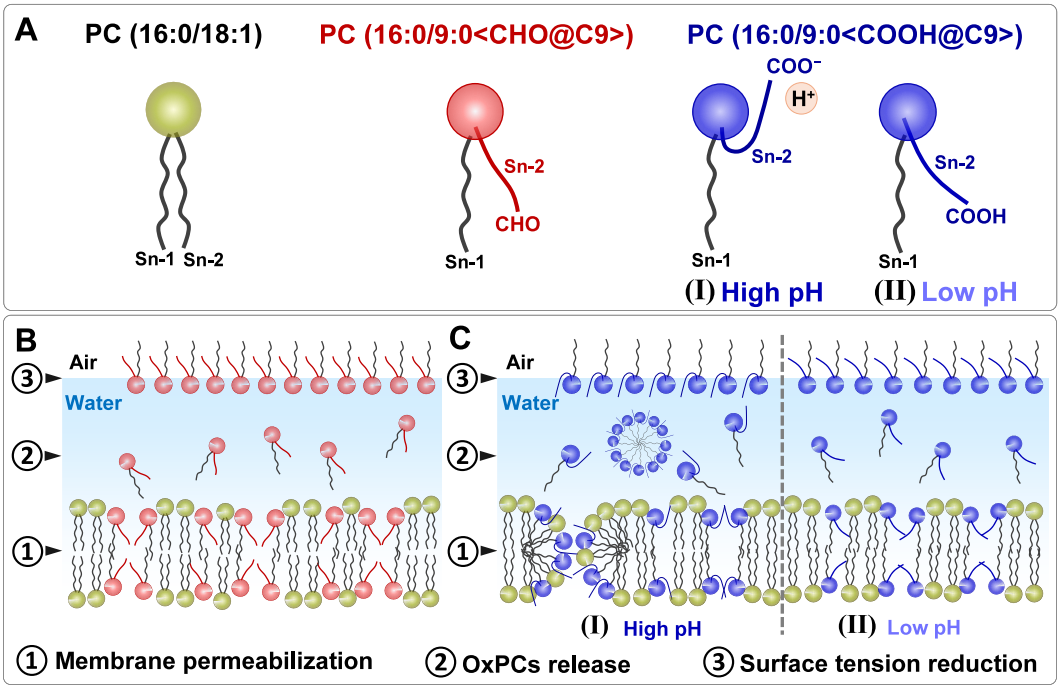

Figure 9. Schematic diagram of effects in membrane bilayers induced by OxPCs with truncated acyl chains. (A) Representations of PC(16:0/18:1), PC(16:0/9:0<CHO@C9>), and PC(16:0/9:0<COOH@C9>) (Top panel). In PC(16:0/9:0<CHO@C9>), the aldehyde function points to the hydrophobic core. At physiological pH (**I**), the carboxylic acid of PC(16:0/9:0<COOH@C9>) is to a large part ionized, and the truncated acyl chain points to the bilayer interface, while at low pH (**II**), the carboxyl function is protonated and points probably to the hydrophobic core in an angle that does not induce high intrinsic molecular curvature.[46] (B) In the presence of PC(16:0/9:0<CHO@C9>), the membrane bilayer becomes more permeable probably because the hydrophilicity of the membrane core is increased by the polar aldehyde groups. At higher concentrations, oxidized lipids might also aggregate and induce diffusion spots. Further, PC(16:0/9:0<CHO@C9>) is probably released from the membrane bilayer and can adsorb at the air−water interface, reducing interfacial tension. (C) In the presence of PC(16:0/9:0<COOH@C9>), (**I**) at high (or neutral) pH, the presence of charged interfacial COO^- functions reduces the ζ-potential and induces high curvature that could induce toroidal pores or transient instabilities due to the formation of isotropic aggregates (probably micelles). The formation of these aggregates could enhance the lipid exchange between bilayer phases and the air−water interface, thereby reducing surface tension more rapidly. (**II**) At low pH, the truncated sn-2 acyl chains point probably to the membrane core which inhibits curvature induction and the formation of isotropic structures, while permeabilization toward SRB is increased, probably by a similar effect observed for PC(16:0/9:0<CHO@C9>).

Similarly, in another study, an increase in flip-flop of NBD-PS was strongly induced by PC(16:0/9:0<COOH@C9>) but less with PC(16:0/9:0<CHO@C9>) at around 10 % mol/mol in a PC(16:0/18:1) bilayer.[50] At these concentrations and because of the setup of their assay,[50] they could exclude permeabilization toward dithionite. Time scales in these experiments were far greater (hours-weeks) than in our assay, but a strong increase of NBD-PS flip-flopping occurred at 14 mol% of PC(16:0/9:0<COOH@C9>) and 16 mol% of PC(16:0/9:0<CHO@C9>), reducing half-life to 1−2 h. At concentrations higher than 20 mol%, they observed permeabilization of the membrane toward dithionite. In our slightly different quenching assay, we observed a threshold of around 12−15 mol% for all truncated lipids tested (Figure 2D,E and Figure S1A,B,C,D). Since our time scales are in the minutes range, a half-life of 1−2 h for flip-flopping would not be detectable, but since we used NBD-PE instead of NBD-PS, flip-flopping might be faster because PE is zwitterionic and has an uncharged small headgroup. We therefore cannot exclude that flip-flopping and/or permeabilization is occurring in the dithionite quenching assay.

In terms of permeabilization thresholds, other studies have seen similar effects for truncated lipids. Runas et al. showed three permeability regimes for PEG12-NBD, a small uncharged hydrophilic molecule of 821 Da, in GUV containing PC(16:0/9:0<CHO@C9>). From 2.5 % to 10 %, permeability increased clearly towards the control, while at concentrations >12.5 %, the bilayer seemed to be disrupted or pores were formed.[51] Thus, the mechanism of permeabilization, and possibly flip-flopping, is dependent on the concentration and the type of oxidized lipids.

When oxidized lipids were added from the outside to the LUVs, there seemed to be no clear threshold at 12−15 mol% since even smaller concentrations induced sulforhodamine B release (Figure 3B,C and Figure S4A,B,C,D). It is possible that the truncated oxidized lipids added from the outside of the LUVs are more concentrated at certain spots of the suspension just after addition and thereby induce permeabilization of a subpopulation of LUVs, although the experiment on GUVs (Figure S2) confirmed that SRB leakage also occurs when the oxidized lipid is present in the membrane at a concentration of 10 mol% which is below the threshold observed for the NBD-PE quenching assay.

At a pH of 7.4, the reduction of surface tension is faster with PC(16:0/9:0<COOH@C9>) than PC(16:0/9:0<CHO@C9>) when the lipid is added to the suspension (Figure 6C,D) and also when the oxidized lipid is released from LUVs (Figure 6C). This means that ionized PC(16:0/9:0<COOH@C9>) is quicker at entering and leaving the monolayer/bilayer than PC(16:0/9:0<CHO@C9>), probably because a higher water solubility of the ionized PC(16:0/9:0<COOH@C9>) goes ahead with a shorter residence time in the bilayer/monolayer.[9] This seems to be confirmed by the fact that a low pH drastically reduces the speed of surface tension reduction by

https://doi.org/10.1021/jacs.4c12543
J. Am. Chem. Soc. 2025, 147, 9175−9189

PC(16:0/9:0<COOH@C9>) (Figure S6). Similarly, it has been shown that, at a pH of 3.0, a monolayer composed of PC(16:0/9:0<COOH@C9>) collapses at a much higher surface pressure than at a pH of 10, meaning that the ionized form of PC(16:0/9:0<COOH@C9>) solubilizes easier in the aqueous phase.[52]

Grauby-Heywang et al. observed the formation of aggregates in the suspension when the monolayer collapsed.[52] We obtained a population of small aggregates, similar in size to micellar structures with PC(16:0/9:0<COOH@C9>) (Figure 5B), which might correspond to the isotropic peak observed in ^{31}P-NMR (Figure 7B). Lipid exchange of bilayers or monolayers with micellar aggregates containing PC(16:0/9:0<COOH@C9>) might also be more rapid. However, permeabilization was faster with PC(16:0/9:0<CHO@C9>) and nonionized PC-(16:0/9:0<COOH@C9>), meaning that the permeabilization rate toward sulforhodamine B relied probably not essentially upon insertion of the lipid into the membrane but on a process that occurs in the membrane.

The fact that oxidized lipids can leave the membrane bilayer and insert at the air−water interface has been observed earlier by our group.[9] This implies that oxidized lipids can not only exert their effects on the cell in which they are produced but also have long-range effects on neighboring cells. Since a reduction of surface tension is observed quite quickly already at small percentages of oxidized lipids (5 mol%), it is possible that the same phenomenon is observed in cells with low amounts of oxidized lipids. The reduction of surface tension is more efficient with PC(16:0/9:0<CHO@C9>) than PC(16:0/9:0<COOH@C9>) at pH = 7.4, probably because the ionized form of PC(16:0/9:0<COOH@C9>) is not likely to accumulate at a high coverage density (surface pressure) and solubilizes more easily in the aqueous phase.[53] Further, PC(16:0/9:0<CHO@C9>) should have a smaller hydrophilic head because its two tails point into the membrane core or air phase (Figure 8). This might result in a larger coverage area at the air−water phase compared to ionized PC(16:0/9:0<COOH@C9>) that points its ionized carboxyl tail to the water phase, thereby increasing the headgroup area (Figure 8 and Figure 9A).[54] This is further supported by the increased surface tension reduction capacity of PC(16:0/9:0<COOH@C9>) at pH = 4.5 where both tails should point to the membrane core or air phase, reducing the headgroup size and increasing coverage (Figure 6E). At acidic pH (4.5), the carboxylic acid functional group is hence less ionized and tends to adopt a molecular conformation similar to PC(16:0/9:0<CHO@C9>) (Figure 9A).

In terms of membranolytic mechanisms, we observed a different picture for aldehyde and carboxylic acids truncated at ΔC5 or ΔC9 (Figure 9). PC(16:0/9:0<COOH@C9>) was able to induce highly curved structures at a pH of 7.4 and beyond (Figure 5B and Figure 7C). In the absence of a high buffer capacity in MLVs and at low pH, these structures were not observed (Figure 7B). Further, the ζ-potential of LUVs containing PC(16:0/9:0<COOH@C9>) decreased with increasing pH (Figure 7D), meaning that PC(16:0/9:0<COOH@C9>) becomes ionized and that its carboxyl function points to the membrane−water interface as was also indicated by our MD simulations (Figure 8B). This behavior has been proposed earlier, but pH dependence has not been shown in liposomes but suggested by MD simulations.[55] The fact that the ionized carboxyl group points to the membrane interface should increase intrinsic molecular curvature of PC(16:0/9:0<COOH@C9>), favoring nonbilayer isotropic aggregates. Permeabilization could hence be induced by the formation of toroidal pores through positive intrinsic molecular curvature, although formation of these pores might require quite high concentrations of PC(16:0/9:0<COOH@C9>).[47,56] The membrane might also simply be destabilized by the formation of micelles and the continuous release of PC(16:0/9:0<COOH@C9>) from the lipid bilayer which might lead to transient instabilities allowing molecules such as dithionite to pass through or increase flip-flopping of NBD-PE. MD simulations show further that the thickness of the membrane is reduced (Figure 8E) with the ionized form of PC(16:0/9:0<COOH@C9>) at high concentrations. This might favor the formation of transient pores and reduce the thickness of the hydrophobic barrier.

When PC(16:0/9:0<COOH@C9>) was less ionized, we observed less curved structures (Figure 7B and Figure S3G), suggesting that the intrinsic molecular curvature of the molecule is reduced.[56] It has been shown in earlier studies that the protonated form of PC(16:0/9:0<COOH@C9>) does not have its truncated acyl chain being pointed to the membrane interface, but rather being in the membrane bilayer, although it is not sure at what membrane depth the protonated COOH group would accumulate.[55] Since there is less formation of isotropic structures, we assume that the intrinsic molecular curvature of the lipid is reduced (Figure 9), suggesting either that the loss of a negative charge at the interface leads to less repulsion of headgroups and carboxyl groups at the membrane interface or the truncated sn-2 acyl chain adopts a conformation that produces less membrane curvature, or both.[20] The permeabilization mechanism might hence be altered and become similar to PC(16:0/9:0<CHO@C9>) whose aldehyde function also remains in the hydrophobic membrane core (Figure 8C) and where no curved structures were observed (Figure 5A and Figure 7A). Ouchi et al. argued that the hydrophobic barrier of the membrane becomes more polar and, hence, more permeable for small hydrophilic molecules, only if the hydrophilic group at the truncation site is pointing to the membrane interior.[48] This might explain why permeabilization toward SRB at low pH was quicker with PC(16:0/9:0<COOH@C9>) than PC(16:0/9:0<CHO@C9>), maybe because of the slightly higher polarity of the COOH function. For the passage of larger and/or charged molecules such as FITC-Dextran, the formation of larger pores would be necessary. It is possible that aggregation of several OxPCs with their aldehyde/nonionized carboxyl function pointing to the membrane interior leads to the formation of larger pores.[48] We did not observe them in our MD simulations, although full pore formation occurs in time scales that are generally not accessible by MD simulations.

Interestingly, high temperatures favored the formation of curved aggregates over bilayers (Figure S7B). It has been proposed for truncated ΔC6 and ΔC12 phospholipids bearing a charged nitrobenzoxadiazole (NBD) group at the truncation site that the conformation of the charged truncated chain depends on the packing of the surrounding bilayer. In a densely packed bilayer environment at low temperature, the NBD group is rather aligned with the acyl chains of other phospholipids, while lower packing at higher temperature promotes the outward conformation.[57,58] A similar behavior of PC(16:0/9:0<COOH@C9>) in membranes would explain the temperature dependent curvature induction. Since headgroup packing is reduced in the presence of truncated OxPCs (Figure 4 and Figure S7A), an increase in their concentrations might thus facilitate the interfacial position of the COOH group.

https://doi.org/10.1021/jacs.4c12543
J. Am. Chem. Soc. 2025, 147, 9175−9189

It seems that some of the effects of PC(16:0/9:0<CHO@C9>) and PC(16:0/9:0<COOH@C9>) are additive (Figure 2F, Figure 3F, Figure S1E, Figure S4F, and Figure S7C,D). This was especially interesting regarding NBD-PE quenching by dithionite since the threshold for individual OxPCs to induce permeabilization or flip-flopping was abolished when a combination of both OxPCs at different molar ratios was used (Figure 2F and Figure S1E). As discussed above, packing defects induced by either of the OxPCs might facilitate the effect of the other OxPCs.[55,59] It is also not clear if both molecules could aggregate to form pores or if mixed lipid aggregates, such as mixed micelles, are formed.

We conclude that the different mechanisms of permeabilization induced by oxidized lipid aldehydes and carboxylic acids depend on a series of parameters (Figure 9), including the pH, ionization state, and the length of the truncated acyl chains.

Physiologically speaking, these results show that permeabilization by truncated carboxylated OxPCs is pH dependent. Upon immune response, macrophages produce ROS at pH=4−5 to kill phagocytosed microorganisms. Since truncated carboxylated lipids are produced in this acid environment, the membrane permeability of these microorganisms might be enhanced and increase the killing efficiency. We recently observed in bacterial membranes that permeabilization at pH = 4.5 upon oxidative stress was stronger.[60] This could indicate that different oxidation products were formed, that acidity itself influences permeabilization, or that permeabilization by OxPCs is enhanced, as we observed here. The release of OxPCs from the membrane is physiologically relevant since certain OxPCs, such as lipid hydroperoxides, have also signaling functions in cells.[61] Truncated OxPCs would thus not need specific transport mechanisms and could simply diffuse to neighboring cells and exert paracrine or membrane destabilizing effects.

Finally, truncated carboxylic OxPCs might be interesting in lipid-based pharmaceutical delivery systems. The ζ-potential of lipid vesicles can be a strong indicator of the stability of the system.[62] In pH-dependent liposomal delivery systems that are used to increase content release in the stomach (pH = 1−4), the intestine (pH = 7−8), or lysosomes (pH = ∼4.5), truncated carboxyls could diminish the negative ζ-potential of vesicles at high pH and increase release of pharmacologically active substances at low pH.

CONCLUSION

We report a systematic investigation on how oxidized lipids with one truncated acyl chain alter properties of membrane bilayers depending on their present concentrations, functional groups, lengths of truncations, and pH. Oxidized lipids with longer truncated tails (ΔC9) are more effective in permeabilizing membranes than those with shorter ones (ΔC5). Lipid aldehydes are likely to permeabilize membrane toward molecules with larger size (e.g., FITC-Dextran and sulforhodamine B) while lipid carboxylic acids tend to permeabilize membrane toward molecules of smaller size or increase lipid flip-flop at neutral pH. At neutral pH, carboxylic acids also induce the formation of highly curved isotropic lipid aggregates and possibly toroidal pores because the ionized carboxyl group protrudes to the membrane interface and induces a high intrinsic molecular curvature. Ionization also seems to favor the release of the lipids from the lipid bilayer and results in a quicker accumulation at the air−water interface. At low pH, the truncated carboxylic acid is nonionized and remains probably inside the hydrophobic core at an angle that prevents the formation of highly curved isotropic structures. However, a low pH of 4.5 increases the capacity of the lipid carboxyl to permeabilize membranes toward larger molecules, similarly to the truncated aldehyde. The mechanism of permeabilization probably depends here on the reduction of the effectiveness of the hydrophobic barrier because of the presence of hydrophilic functions inside the membrane or the formation of nontoroidal pores.

Our work provides a whole picture of membranolytic effects of truncated oxidized lipids, which could help to understand the effects of these lipids on biological cell membranes. We further describe the possibility of a paracrine effect of these lipids on neighboring cells and the usefulness of truncated carboxylated lipids in the design of pH-dependent drug delivery systems.

ASSOCIATED CONTENT

Supporting Information

The Supporting Information is available free of charge at https://pubs.acs.org/doi/10.1021/jacs.4c12543.

Computational and experimental materials and methods; additional data for membrane permeabilization, Cryo-EM imaging, membrane packing, surface tension reduction, and ^{31}P-NMR analysis (PDF)

AUTHOR INFORMATION

Corresponding Author

Joseph H. Lorent − *Membrane Biochemistry & Biophysics, Bijvoet Center for Biomolecular Research, Department of Chemistry, Utrecht University, 3584 CH Utrecht, The Netherlands; Cellular and Molecular Pharmacology, Translational Research from Experimental and Clinical Pharmacology to Treatment Optimization, Louvain Drug Research Institute, UCLouvain, B-1200 Brussels, Belgium;* orcid.org/0000-0002-7537-8521; Email: joseph.lorent@uclouvain.be

Authors

Min Xie − *Membrane Biochemistry & Biophysics, Bijvoet Center for Biomolecular Research, Department of Chemistry, Utrecht University, 3584 CH Utrecht, The Netherlands;* orcid.org/0009-0002-2828-8096

Maik G. N. Derks − *Membrane Biochemistry & Biophysics, Bijvoet Center for Biomolecular Research, Department of Chemistry, Utrecht University, 3584 CH Utrecht, The Netherlands; Nuclear Magnetic Resonance Spectroscopy, Bijvoet Center for Biomolecular Research, Department of Chemistry, Utrecht University, 3584 CH Utrecht, The Netherlands;* orcid.org/0000-0001-8962-5362

Eveline H. W. Koch − *Membrane Biochemistry & Biophysics, Bijvoet Center for Biomolecular Research, Department of Chemistry, Utrecht University, 3584 CH Utrecht, The Netherlands;* orcid.org/0009-0004-3432-2910

C. Bjorn van Boven − *Membrane Biochemistry & Biophysics, Bijvoet Center for Biomolecular Research, Department of Chemistry, Utrecht University, 3584 CH Utrecht, The Netherlands*

Minchakarn Janlad − *Department of Physics, Faculty of Science, Kasetsart University, Bangkok 10900, Thailand; Computational Biomodelling Laboratory for Agricultural Science and Technology (CBLAST), Faculty of Science, Kasetsart University, Bangkok 10900, Thailand*

https://doi.org/10.1021/jacs.4c12543
J. Am. Chem. Soc. 2025, 147, 9175−9189

Behnaz Bagheri − *Department of Applied Physics and Science Education, Technical University of Eindhoven, Eindhoven 5600 MB, The Netherlands; Institute for Complex Molecular Systems, Eindhoven 5600 MB, The Netherlands*
Zexi Xu − *Membrane Biochemistry & Biophysics, Bijvoet Center for Biomolecular Research, Department of Chemistry, Utrecht University, 3584 CH Utrecht, The Netherlands*
Daria Kovryzhenko − *Cellular and Molecular Pharmacology, Translational Research from Experimental and Clinical Pharmacology to Treatment Optimization, Louvain Drug Research Institute, UCLouvain, B-1200 Brussels, Belgium*
Cornelis A. van Walree − *Membrane Biochemistry & Biophysics, Bijvoet Center for Biomolecular Research, Department of Chemistry, Utrecht University, 3584 CH Utrecht, The Netherlands; University College Utrecht, 3584 ED Utrecht, The Netherlands;* orcid.org/0000-0002-6178-1424
Ana Sobota − *Department of Applied Physics and Science Education, Eindhoven University of Technology, 5600 MB Eindhoven, The Netherlands*
Markus Weingarth − *Nuclear Magnetic Resonance Spectroscopy, Bijvoet Center for Biomolecular Research, Department of Chemistry, Utrecht University, 3584 CH Utrecht, The Netherlands;* orcid.org/0000-0003-0831-8673
Jirasak Wong-ekkabut − *Department of Physics, Faculty of Science, Kasetsart University, Bangkok 10900, Thailand; Computational Biomodelling Laboratory for Agricultural Science and Technology (CBLAST), Faculty of Science, Kasetsart University, Bangkok 10900, Thailand*
Mikko Karttunen − *Department of Chemistry, Western University, London, Ontario N6A 5B7, Canada; Department of Physics and Astronomy, Western University, London, Ontario N6A 3K7, Canada;* orcid.org/0000-0002-8626-3033
Eefjan Breukink − *Membrane Biochemistry & Biophysics, Bijvoet Center for Biomolecular Research, Department of Chemistry, Utrecht University, 3584 CH Utrecht, The Netherlands;* orcid.org/0000-0002-7311-0660
J. Antoinette Killian − *Membrane Biochemistry & Biophysics, Bijvoet Center for Biomolecular Research, Department of Chemistry, Utrecht University, 3584 CH Utrecht, The Netherlands*
Andreas F. P. Sonnen − *Pathology Department, University Medical Center Utrecht, 3508 GA Utrecht, The Netherlands*

Complete contact information is available at: https://pubs.acs.org/10.1021/jacs.4c12543

Notes

The authors declare no competing financial interest.

■ ACKNOWLEDGMENTS

We are grateful to Bonny W. M. Kuipers for support in DLS analysis and Martin F. Haase for providing pendant drop tensiometer equipment. We further thank the Alliance of Utrecht University and Eindhoven University of Technology (grant number BG.180191.4.09) for financing this project. M.X. was supported by a scholarship from the China Scholarship Council (CSC), https://www.csc.edu.cn/, file no. 201809370077. M.K. thanks the Canada Research Chairs Program and the Natural Sciences and Engineering Research Council of Canada (NSERC) for financial support. J.W. is supported by the National Science Research and Innovation fund (NSRF) via the Program Management Unit for Human Resources and Institutional Development, Research and Innovation [grant numberB42G670041]. J.H.L. thanks the Fédération Wallonie-Bruxelles (grant number 24/29-143) for financial support. The authors also thank the Digital Research Alliance of Canada for computational resources.

■ REFERENCES

(1) Byrns, C. N.; Perlegos, A. E.; Miller, K. N.; Jin, Z.; Carranza, F. R.; Manchandra, P.; Beveridge, C. H.; Randolph, C. E.; Chaluvadi, V. S.; Zhang, S. L.; Srinivasan, A. R.; Bennett, F. C.; Sehgal, A.; Adams, P. D.; Chopra, G.; Bonini, N. M. Senescent Glia Link Mitochondrial Dysfunction and Lipid Accumulation. *Nature 2024 630:8016* **2024**, *630* (8016), 475−483.
(2) Yoritaka, A.; Hattori, N.; Uchida, K.; Tanaka, M.; Stadtman, E. R.; Mizuno, Y. Immunohistochemical Detection of 4-Hydroxynonenal Protein Adducts in Parkinson Disease. *Proc. Natl. Acad. Sci. U. S. A.* **1996**, *93* (7), 2696−2701.
(3) Sanyal, J.; Bandyopadhyay, S. K.; Banerjee, T. K.; Mukherjee, S. C.; Chakraborty, D. P.; Ray, B. C.; Rao, V. R. Plasma Levels of Lipid Peroxides in Patients with Parkinson's Disease. *Eur. Rev. Med. Pharmacol Sci.* **2009**, *13* (2), 129−132.
(4) Navarro, A.; Boveris, A.; Bández, M. J.; Sánchez-Pino, M. J.; Gómez, C.; Muntané, G.; Ferrer, I. Human Brain Cortex: Mitochondrial Oxidative Damage and Adaptive Response in Parkinson Disease and in Dementia with Lewy Bodies. *Free Radic Biol. Med.* **2009**, *46* (12), 1574−1580.
(5) Valko, M.; Leibfritz, D.; Moncol, J.; Cronin, M. T. D.; Mazur, M.; Telser, J. Free Radicals and Antioxidants in Normal Physiological Functions and Human Disease. *Int. J. Biochem. Cell Biol.* **2007**, *39* (1), 44−84.
(6) Negre-Salvayre, A.; Auge, N.; Ayala, V.; Basaga, H.; Boada, J.; Brenke, R.; Chapple, S.; Cohen, G.; Feher, J.; Grune, T.; Lengyel, G.; Mann, G. E.; Pamplona, R.; Poli, G.; Portero-Otin, M.; Riahi, Y.; Salvayre, R.; Sasson, S.; Serrano, J.; Shamni, O.; Siems, W.; Siow, R. C. M.; Wiswedel, I.; Zarkovic, K.; Zarkovic, N. Pathological Aspects of Lipid Peroxidation. *Free Radic Res.* **2010**, *44* (10), 1125−1171.
(7) Wang, C.-H.; Chang, R.-W.; Ko, Y.-H.; Tsai, P.-R.; Wang, S.-S.; Chen, Y.-S.; Ko, W.-J.; Chang, C.-Y.; Young, T.-H.; Chang, K.-C. Prevention of Arterial Stiffening by Using Low-Dose Atorvastatin in Diabetes Is Associated with Decreased Malondialdehyde. *PLoS One* **2014**, *9* (3), No. e90471.
(8) Cristalli, D. O.; Arnal, N.; Marra, F. A.; de Alaniz, M. J. T.; Marra, C. A. Peripheral Markers in Neurodegenerative Patients and Their First-Degree Relatives. *J. Neurol Sci.* **2012**, *314* (1−2), 48−56.
(9) Xie, M.; Koch, E. H. W.; van Walree, C. A.; Sobota, A.; Sonnen, A. F. P.; Breukink, E.; Killian, J. A.; Lorent, J. H. Two Separate Mechanisms Are Involved in Membrane Permeabilization during Lipid Oxidation. *Biophys. J.* **2023**, *122* (23), 4503.
(10) Murphy, M. P. How Mitochondria Produce Reactive Oxygen Species. *Biochem. J.* **2009**, *417* (1), 1−13.
(11) Ayala, A.; Muñoz, M. F.; Argüelles, S. Lipid Peroxidation: Production, Metabolism, and Signaling Mechanisms of Malondialdehyde and 4-Hydroxy-2-Nonenal. *Oxid Med. Cell Longev* **2014**, *2014*, 360438.
(12) Altan, O.; Pabuçcuoğlu, A.; Altan, A.; Konyalioğlu, S.; Bayraktar, H. Effect of Heat Stress on Oxidative Stress, Lipid Peroxidation and Some Stress Parameters in Broilers. *Br Poult Sci.* **2003**, *44* (4), 545−550.
(13) Spickett, C. M. Formation of Oxidatively Modified Lipids as the Basis for a Cellular Epilipidome. *Front Endocrinol (Lausanne)* **2020**, *11*, 1−8.
(14) Hutchins, P. M.; Moore, E. E.; Murphy, R. C. Electrospray MS/MS Reveals Extensive and Nonspecific Oxidation of Cholesterol Esters in Human Peripheral Vascular Lesions[S]. *J. Lipid Res.* **2011**, *52* (11), 2070−2083.

(15) Guo, S.; Lu, J.; Zhuo, Y.; Xiao, M.; Xue, X.; Zhong, S.; Shen, X.; Yin, C.; Li, L.; Chen, Q.; Zhu, M.; Chen, B.; Zhao, M.; Zheng, L.; Tao, Y.; Yin, H. Endogenous Cholesterol Ester Hydroperoxides Modulate Cholesterol Levels and Inhibit Cholesterol Uptake in Hepatocytes and Macrophages. *Redox Biol.* **2019**, *21*, 101069.
(16) Guéraud, F.; Atalay, M.; Bresgen, N.; Cipak, A.; Eckl, P. M.; Huc, L.; Jouanin, I.; Siems, W.; Uchida, K. Chemistry and Biochemistry of Lipid Peroxidation Products. *Free Radic Res.* **2010**, *44* (10), 1098−1124.
(17) Sousa, B. C.; Pitt, A. R.; Spickett, C. M. Chemistry and Analysis of HNE and Other Prominent Carbonyl-Containing Lipid Oxidation Compounds. *Free Radic Biol. Med.* **2017**, *111*, 294−308.
(18) Reis, A.; Spickett, C. M. Chemistry of Phospholipid Oxidation. *Biochim Biophys Acta Biomembr* **2012**, *1818* (10), 2374−2387.
(19) Jurkiewicz, P.; Cwiklik, L.; Jungwirth, P.; Hof, M. Lipid Hydration and Mobility: An Interplay between Fluorescence Solvent Relaxation Experiments and Molecular Dynamics Simulations. *Biochimie.* **2012**, *94* (1), 26−32.
(20) Israelachvili, J. *Intermolecular and Surface Forces*, Third ed.; Academic Press, 2011; DOI: 10.1016/C2009-0-21560-1.
(21) Singer, S. J.; Nicolson, G. L. The Structure and Chemistry of Mammalian Cell Membranes. *Am. J. Pathol.* **1971**, *65* (2), 427−437.
(22) Rosa, R. De; Spinozzi, F.; Itri, R. Hydroperoxide and Carboxyl Groups Preferential Location in Oxidized Biomembranes Experimentally Determined by Small Angle X-Ray Scattering: Implications in Membrane Structure. *Biochim Biophys Acta Biomembr* **2018**, *1860* (11), 2299−2307.
(23) Wong-Ekkabut, J.; Xu, Z.; Triampo, W.; Tang, I. M.; Tieleman, D. P.; Monticelli, L. Effect of Lipid Peroxidation on the Properties of Lipid Bilayers: A Molecular Dynamics Study. *Biophys. J.* **2007**, *93* (12), 4225−4236.
(24) Khandelia, H.; Mouritsen, O. G. Lipid Gymnastics: Evidence of Complete Acyl Chain Reversal in Oxidized Phospholipids from Molecular Simulations. *Biophys. J.* **2009**, *96* (7), 2734−2743.
(25) Bagheri, B.; Boonnoy, P.; Wong-Ekkabut, J.; Karttunen, M. Effect of Oxidation on POPC Lipid Bilayers: Anionic Carboxyl Group Plays a Major Role. *Phys. Chem. Chem. Phys.* **2023**, *25* (27), 18310−18321.
(26) Bour, A.; Kruglik, S. G.; Chabanon, M.; Rangamani, P.; Puff, N.; Bonneau, S. Lipid Unsaturation Properties Govern the Sensitivity of Membranes to Photoinduced Oxidative Stress. *Biophys. J.* **2019**, *116* (5), 910−920.
(27) Parra-Ortiz, E.; Browning, K. L.; Damgaard, L. S. E.; Nordström, R.; Micciulla, S.; Bucciarelli, S.; Malmsten, M. Effects of Oxidation on the Physicochemical Properties of Polyunsaturated Lipid Membranes. *J. Colloid Interface Sci.* **2019**, *538*, 404−419.
(28) Boonnoy, P.; Jarerattanachat, V.; Karttunen, M.; Wong-Ekkabut, J. Bilayer Deformation, Pores, and Micellation Induced by Oxidized Lipids. *J. Phys. Chem. Lett.* **2015**, *6* (24), 4884−4888.
(29) Heuvingh, J.; Bonneau, S. Asymmetric Oxidation of Giant Vesicles Triggers Curvature-Associated Shape Transition and Permeabilization. *Biophys. J.* **2009**, *97* (11), 2904−2912.
(30) Yusupov, M.; Van der Paal, J.; Neyts, E. C.; Bogaerts, A. Synergistic Effect of Electric Field and Lipid Oxidation on the Permeability of Cell Membranes. *Biochim Biophys Acta Gen Subj* **2017**, *1861* (4), 839−847.
(31) Mertins, O.; Bacellar, I. O. L.; Thalmann, F.; Marques, C. M.; Baptista, M. S.; Itri, R. Physical Damage on Giant Vesicles Membrane as a Result of Methylene Blue Photoirradiation. *Biophys. J.* **2014**, *106* (1), 162−171.
(32) Tsubone, T. M.; Junqueira, H. C.; Baptista, M. S.; Itri, R. Contrasting Roles of Oxidized Lipids in Modulating Membrane Microdomains. *Biochim Biophys Acta Biomembr* **2019**, *1861* (3), 660−669.
(33) Runas, K. A.; Acharya, S. J.; Schmidt, J. J.; Malmstadt, N. Addition of Cleaved Tail Fragments during Lipid Oxidation Stabilizes Membrane Permeability Behavior. *Langmuir* **2016**, *32* (3), 779−786.
(34) Bagheri, B.; Boonnoy, P.; Wong-Ekkabut, J.; Karttunen, M. Effect of Oxidation on POPC Lipid Bilayers: Anionic Carboxyl Group Plays a Major Role. *Phys. Chem. Chem. Phys.* **2023**, *25* (27), 18310−18321.
(35) Parasassi, T.; De Stasio, G.; d'Ubaldo, A.; Gratton, E. Phase Fluctuation in Phospholipid Membranes Revealed by Laurdan Fluorescence. *Biophys. J.* **1990**, *57* (6), 1179−1186.
(36) Lorent, J. H.; Levental, K. R.; Ganesan, L.; Rivera-Longsworth, G.; Sezgin, E.; Doktorova, M.; Lyman, E.; Levental, I. Plasma Membranes Are Asymmetric in Lipid Unsaturation, Packing and Protein Shape. *Nat. Chem. Biol.* **2020**, *16* (6), 644−652.
(37) Suhaj, A.; Gowland, D.; Bonini, N.; Owen, D. M.; Lorenz, C. D. Laurdan and Di-4-ANEPPDHQ Influence the Properties of Lipid Membranes: A Classical Molecular Dynamics and Fluorescence Study. *J. Phys. Chem. B* **2020**, *124* (50), 11419−11430.
(38) Bacalum, M.; Zorila, B.; Radu, M. Fluorescence Spectra Decomposition by Asymmetric Functions: Laurdan Spectrum Revisited. *Anal. Biochem.* **2013**, *440* (2), 123−129.
(39) Sousa, T.; Castro, R. E.; Coutinho, A.; Rodrigues, C. M. P.; Prieto, M.; Fernandes, F. *Measuring the Impact of Bile Acids on the Membrane Order of Primary Hepatocytes and Isolated Mitochondria by Fluorescence Imaging and Spectroscopy BT - Experimental Cholestasis Research*; Vinken, M., Ed.; Springer New York: New York, NY, 2019; pp 99−115; DOI: 10.1007/978-1-4939-9420-5_7.
(40) Brown, R. E.; Brockman, H. L. Using Monomolecular Films to Characterize Lipid Lateral Interactions. *Lipid Rafts* **2007**, *398*, 41−58.
(41) Mukherjee, I.; Moulik, S. P.; Rakshit, A. K. Tensiometric Determination of Gibbs Surface Excess and Micelle Point: A Critical Revisit. *J. Colloid Interface Sci.* **2013**, *394* (1), 329−336.
(42) Zhao, J.; Dai, C.; Ding, Q.; Du, M.; Feng, H.; Wei, Z.; Chen, A.; Zhao, M. The Structure Effect on the Surface and Interfacial Properties of Zwitterionic Sulfobetaine Surfactants for Enhanced Oil Recovery. *RSC Adv.* **2015**, *5* (18), 13993−14001.
(43) Qiao, L.; Ge, A.; Liang, Y.; Ye, S. Oxidative Degradation of the Monolayer of 1-Palmitoyl-2-Oleoyl-Sn-Glycero-3-Phosphocholine (POPC) in Low-Level Ozone. *J. Phys. Chem. B* **2015**, *119* (44), 14188−14199.
(44) Gröbner, G.; Williamson, P. Solid-State NMR Methods for Studying Membrane Systems. In *Solid-State NMR*; IOP Publishing, 2020; pp 1-1−1-30; DOI: 10.1088/978-0-7503-2532-5ch1.
(45) McLaughlin, A. C.; Cullis, P. R.; Berden, J. A.; Richards, R. E. 31P NMR of Phospholipid Membranes: Effects of Chemical and Anisotropy at High Magnetic Field Strengths. *Journal of Magnetic Resonance (1969)* **1975**, *20* (1), 146−165.
(46) Mendes Ferreira, T.; Bärenwald, R.; Sood, R.; Volinsky, R.; Drescher, S.; Karlström, G.; Topgaard, D.; Kinnunen, P.; Saalwächter, K.; Ollila, S. Oxidized Lipids in Model Membranes: Atomistic Details from Solid-State NMR Experiments and MD Simulations. *Biophys. J.* **2016**, *110* (3), 584a.
(47) Jurkiewicz, P.; Olzyńska, A.; Cwiklik, L.; Conte, E.; Jungwirth, P.; Megli, F. M.; Hof, M. Biophysics of Lipid Bilayers Containing Oxidatively Modified Phospholipids: Insights from Fluorescence and EPR Experiments and from MD Simulations. *Biochimica et Biophysica Acta - Biomembranes* **2012**, *1818*, 2388−2402.
(48) Ouchi, Y.; Unoura, K.; Nabika, H. Role of Oxidized Lipids in Permeation of H2O2 Through a Lipid Membrane: Molecular Mechanism of an Inhibitor to Promoter Switch. *Sci. Rep* **2019**, *9* (1), 1−4.
(49) Sandrin, D.; Wagner, D.; Sitta, C. E.; Thoma, R.; Felekyan, S.; Hermes, H. E.; Janiak, C.; De Sousa Amadeu, N.; Kühnemuth, R.; Löwen, H.; Egelhaaf, S. U.; Seidel, C. A. M. Diffusion of Macromolecules in a Polymer Hydrogel: From Microscopic to Macroscopic Scales. *Phys. Chem. Chem. Phys.* **2016**, *18* (18), 12860−12876.
(50) Volinsky, R.; Cwiklik, L.; Jurkiewicz, P.; Hof, M.; Jungwirth, P.; Kinnunen, P. K. J. Oxidized Phosphatidylcholines Facilitate Phospholipid Flip-Flop in Liposomes. *Biophys. J.* **2011**, *101* (6), 1376−1384.
(51) Runas, K. A.; Malmstadt, N. Low Levels of Lipid Oxidation Radically Increase the Passive Permeability of Lipid Bilayers. *Soft Matter* **2015**, *11* (3), 499−505.
(52) Grauby-Heywang, C.; Moroté, F.; Mathelié-Guinlet, M.; Gammoudi, I.; Faye, N. R.; Cohen-Bouhacina, T. Influence of Oxidized Lipids on Palmitoyl-Oleoyl-Phosphatidylcholine Organization, Con-

https://doi.org/10.1021/jacs.4c12543
J. Am. Chem. Soc. 2025, 147, 9175−9189

tribution of Langmuir Monolayers and Langmuir-Blodgett Films. *Chem. Phys. Lipids* **2016**, *200*, 74−82.
(53) Grauby-Heywang, C.; Moroté, F.; Mathelié-Guinlet, M.; Gammoudi, I.; Faye, N. R.; Cohen-Bouhacina, T. Influence of Oxidized Lipids on Palmitoyl-Oleoyl-Phosphatidylcholine Organization, Contribution of Langmuir Monolayers and Langmuir-Blodgett Films. *Chem. Phys. Lipids* **2016**, *200*, 74−82.
(54) Czajka, A.; Hazell, G.; Eastoe, J. Surfactants at the Design Limit. *Langmuir* **2015**, *31* (30), 8205−8217.
(55) Mendes Ferreira, T.; Sood, R.; Bärenwald, R.; Carlström, G.; Topgaard, D.; Saalwächter, K.; Kinnunen, P. K. J.; Ollila, O. H. S. Acyl Chain Disorder and Azelaoyl Orientation in Lipid Membranes Containing Oxidized Lipids. *Langmuir* **2016**, *32* (25), 6524−6533.
(56) Lorent, J.; Le Duff, C. S.; Quetin-Leclercq, J.; Mingeot-Leclercq, M.-P. Induction of Highly Curved Structures in Relation to Membrane Permeabilization and Budding by the Triterpenoid Saponins, Alpha- and Delta-Hederin. *J. Biol. Chem.* **2013**, *288* (20), 14000−14017.
(57) Stockl, M.; Plazzo, A. P.; Korte, T.; Herrmann, A. Detection of Lipid Domains in Model and Cell Membranes by Fluorescence Lifetime Imaging Microscopy of Fluorescent Lipid Analogues. *J. Biol. Chem.* **2008**, *283* (45), 30828−30837.
(58) Filipe, H. A. L.; Pokorná, Š.; Hof, M.; Amaro, M.; Loura, L. M. S. Orientation of Nitro-Group Governs the Fluorescence Lifetime of Nitrobenzoxadiazole (NBD)-Labeled Lipids in Lipid Bilayers. *Phys. Chem. Chem. Phys.* **2019**, *21* (4), 1682−1688.
(59) Megli, F. M.; Conte, E.; Russo, L. Comparative 5-Doxylstearoyllecithin and 3-Doxylcholestane EPR Spin Labeling Study of Phospholipid Bilayer Perturbation by Different Oxidized Lecithin Species. *Biochim Biophys Acta Biomembr* **2010**, *1798* (1), 1886−1898.
(60) Xie, M.; Koch, E. H. W.; van Walree, C. A.; Sobota, A.; Sonnen, A. F. P.; Killian, J. A.; Breukink, E.; Lorent, J. H. Synergistic Effects of Oxidative and Acid Stress on Bacterial Membranes of Escherichia Coli and Staphylococcus Simulans. *Commun. Biol.* **2024**, *7* (1), 1161.
(61) Korytowski, W.; Basova, L. V.; Pilat, A.; Kernstock, R. M.; Girotti, A. W. Permeabilization of the Mitochondrial Outer Membrane by Bax/Truncated Bid (TBid) Proteins as Sensitized by Cardiolipin Hydroperoxide Translocation: Mechanistic Implications for the Intrinsic Pathway of Oxidative Apoptosis. *J. Biol. Chem.* **2011**, *286* (30), 26334−26343.
(62) Smith, M. C.; Crist, R. M.; Clogston, J. D.; McNeil, S. E. Zeta Potential: A Case Study of Cationic, Anionic, and Neutral Liposomes. *Anal Bioanal Chem.* **2017**, *409* (24), 5779−5787.

https://doi.org/10.1021/jacs.4c12543
J. Am. Chem. Soc. 2025, 147, 9175−9189

Supporting Information

Structure and pH-dependence of membranolytic mechanisms by truncated oxidized phospholipids

Min Xie[1], Maik G. N. Derks[1,2], Eveline H. W. Koch[1], C. Bjorn van Boven[1], Minchakarn Janlad[11,12], Behnaz Bagheri[7,8], Zexi Xu[1], Daria Kovryzhenko[6], Cornelis A. van Walree[1,3], Ana Sobota[4], Markus Weingarth[2], Jirasak Wong-ekkabut[11,12], Mikko Karttunen[9,10], Eefjan Breukink[1], J. Antoinette Killian[1], Andreas F. P. Sonnen[1,5] and Joseph H. Lorent[1,6,*]

[1]Membrane Biochemistry & Biophysics, Bijvoet Center for Biomolecular Research, Department of Chemistry, Utrecht University, Padualaan 8, 3584 CH Utrecht, the Netherlands

[2]Nuclear Magnetic Resonance Spectroscopy, Bijvoet Center for Biomolecular Research, Department of Chemistry, Utrecht University, Padualaan 8, 3584 CH Utrecht, the Netherlands

[3]University College Utrecht, Campusplein 1, 3584 ED Utrecht, the Netherlands

[4]Atmospheric Pressure Non-Thermal Plasmas and their Interaction with Targets, Applied Physics Department, Eindhoven University of Technology, 5600 MB Eindhoven, the Netherlands

[5]Pathology Department, University Medical Center Utrecht, Heidelberglaan 100, H04.312, Postbus 85500, 3508 GA Utrecht, the Netherlands

[6]Cellular and Molecular Pharmacology, Translational Research from Experimental and Clinical Pharmacology to Treatment Optimization, Louvain Drug Research Institute, UCLouvain, Avenue Mounier 73+1, B1.73.05, B-1200 Brussels, Belgium

[7]Department of Applied Physics and Science Education, Technical University of Eindhoven, PO Box 513, Eindhoven, 5600 MB, the Netherlands

[8]Institute for Complex Molecular Systems, PO Box 513, Eindhoven, 5600 MB, the Netherlands

[9]Department of Chemistry, Western University, 1151 Richmond Street, London, Ontario, N6A 5B7, Canada

[10]Department of Physics and Astronomy, Western University, 1151 Richmond Street, London, Ontario, N6A 3K7, Canada

[11]Department of Physics, Faculty of Science, Kasetsart University, 50 Ngamwongwan Rd., Chatuchak, Bangkok 10900, Thailand

[12]Computational Biomodelling Laboratory for Agricultural Science and Technology (CBLAST), Faculty of Science, Kasetsart University, 50 Ngamwongwan Rd., Chatuchak, Bangkok, 10900, Thailand

*Corresponding author: joseph.lorent@uclouvain.be

Content

1. Materials and methods

1.1 Chemicals and reagents

1-palmitoyl-2-oleoyl-glycero-3-phosphocholine (PC(16:0/18:1), POPC), 1-palmitoyl-2-(9'-oxo-nonanoyl)-sn-glycero-3-phosphocholine (PC(16:0/9:0<CHO@C9>), ALDOPC), 1-palmitoyl-2-azelaoyl-sn-glycero-3-phosphocholine (PC(16:0/9:0<COOH@C9>), PAzePC), 1-palmitoyl-2-(5'-oxo-valeroyl)-sn-glycero-3-phosphocholine (PC(16:0/5:0<CHO@C5>), POVPC), 1-palmitoyl-2-glutaryl-sn-glycero-3-phosphocholine (PC(16:0/5:0<COOH@C5>), PGPC) and 1,2-dioleoyl-sn-glycero-3-phosphoethanolamine-N-(7-nitro-2-1,3-benzoxadiazol-4-yl) (ammonium salt) (NBD-PE (18:1/18:1)) were purchased from Avanti Polar Lipids (USA). Laurdan (6-Dodecanoyl-2-Dimethylaminonaphthalene) and di-4-ANEPPDHQ were ordered from Thermo Fisher Scientific (US). DPH (Diphenylhexatriene), FITC-Dextran (4kDa), sodium dithionite and sulforhodamine B were ordered from Merck (USA).

1.2 Preparation of large unilamellar vesicles (LUVs)

Stock lipid solutions were prepared in chloroform and corresponding volumes of PC(16:0/18:1) alone or mixed with oxidized and fluorescent lipids were added into a glass tube and dried under a nitrogen stream at room temperature. Solvent remnants were further eliminated in a vacuum chamber for at least 1 hour. Afterwards, a certain amount of aqueous solution (depending on specific experimental conditions) was added to the lipid film and the suspension was heated above the transition temperature of the lipids in warm water (at around 40 °C) bath for 30 minutes. Afterwards, the hydrated lipid suspension underwent 10 cycles of freezing-thawing process between dry ice (in ethanol) and the warm water, and each process was around 3 minutes. The formed multilamellar vesicles (MLVs) were extruded with an extruder (Avanti polar lipids) and filters of 200 nm, resulting in LUVs with diameter at around 200 nm.

1.3 Preparation of giant unilamellar vesicles (GUVs)

GUVs were made by the agarose assisted swelling method[1]. We used pure PC(16:0/18:1) as control, while other samples contained 80 mol% of PC(16:0/18:1) and 20 mol% of either PC(16:0/9:0<CHO@C9>) or PC(16:0/9:0<COOH@C9>). All GUVs were labeled with 0.1 mol% of rhodamine B-PE (18:1/18:1). Specifically, 1 ml of 1 mg/ml agarose gel (at around 60°C, ultra-pure, Sigma-Aldrich) was added into a glass tube which was cleaned with isopropanol before use. The glass tube with warm agarose gel was placed at room temperature for 3 minutes, whereafter the liquid agarose was removed using a pipette. The formed agarose gel film was further dried with a rotavapor for 30 minutes at 40°C (in water bath) at 90 rpm. One hundred microliters of lipid mixture (in chloroform, 0.5 mg/ml) were added into the glass tube with the dried agarose gel. The lipid solution was evaporated in the rotavapor at room temperature and 90 rpm for at least 60 minutes. Five hundred microliters of 0.3 M sucrose was added to hydrate the lipid film and placed in the dark for 3-4 hours at ambient temperature to allow for swelling of GUV. Finally, 30 microliters of the GUV suspension was observed by confocal microscopy in IBIDI chambers containing 300 µl of 0.3 M glucose with FITC-Dextran solution (freshly made in Milli-Q-H_2O) after a 10 min incubation period. The final concentration of FITC-Dextran was 40 µM.

For the sulforhodamine leakage assay, we used the same approach as described above but used NBD-PE to stain the GUVs (0.1 %) and a sucrose solution of 0.1M to hydrate GUVs. To image GUV permeabilization, we used 50 µl of GUV suspension that was added to 250 µl sulforhodamine B solution at 10 µM concentration in a phosphate buffer adjusted to 0.1 M at pH=7.4. GUVs were imaged after 2 h incubation.

1.4 Imaging permeabilization of GUVs with confocal microscopy

GUVs stained with Rhodamine B-PE or NBD-PE floating either in a FITC-Dextran (4 kDa) or sulforhodamine B suspension, respectively, were imaged by confocal microscopy. Excitation for (Rhodamine/Rhodamine-PE) was done at 555 nm while it was recorded at 580 nm. NBD-PE and FITC-dextran were visualized by excitation at 488 nm and recording at 523 nm. For imaging, we used a confocal microscope, LSM 700, AxioObserver with an EC Plan-Neofluar 40×1.30 Oil DIC M27 objective, and images were recorded with a high-resolution AxioCam microscope camera.

All GUV images were processed with ImageJ (a public domain Java image processing program, https://imagej.nih.gov/ij/) and Matlab®. Average fluorescence intensity was determined inside individual GUVs, and an average outside fluorescence intensity was determined. Permeabilization in percentage was calculated per GUV as: *% Permeabilization = Mean FI (inside GUV) / Mean FI (outside GUV) × 100 %.*

1.5. Cryo-EM imaging

Different liposome preparations were plunge frozen in liquid ethane using a home-made plunge freezer under high humidity. EM grids were stored in liquid nitrogen until imaging under cryo conditions using a Thermofisher Talos Arctica at 200 kV under low-dose conditions using a Gatan K2 direct-electron detector and a magnification of 63000x (0,221 nm/pixel). Overview maps of suitable grid squares were taken at 7300 x magnification. Percent multilamellarity was determined by acquiring grid square maps and counting at least 250 vesicles and determining whether they were multilamellar. At the same time the diameter was measured. Images in which vesicles clearly were frozen on-top of each other were not counted as multilamellar. Diameter was only measured of non-deformed liposomes. In all samples a similar percentage of approximately 4 % multilamellarity was seen.

1.6 Dithionite quenching assay

PC(16:0/18:1) LUVs were incorporated with different fractions of OxPCs and prepared as described above. For dithionite quenching assay, 0.5 mol% of headgroup labelled NBD-PE (18:1/18:1) was added to the lipid film. Afterwards, 400 mM KCl solution was used to hydrate the lipid film. LUVs were further diluted with PBS (38.38 mM Na_2HPO_4 and 19.62 mM NaH_2PO_4, NaCl 334.8 mM, pH 7.4) to a final concentration at 100 µM. 1 ml of LUVs suspension at 100 µM was added into the cuvette with a stirring bar inside for agitation. The fluorescence intensity of the NBD fluorophore was recorded from time zero (T_0 min) with an excitation and emission wavelength at 488 nm and 520 nm, respectively. At T_2 min, dithionite was added into the LUVs suspension to a final concentration of 10 mM (**Figure 2C**), and at T_8 min, Triton X-100 was added to reach a concentration of 0.1%. The experiment was performed at 20 °C.

1.7 Sulforhodamine B leakage assay

One milliliter of 20 mM stock solution PC(16:0/18:1) in $CHCl_3$ was dried under nitrogen stream and remnant solvent was further eliminated in vacuum for 60 minutes. Sulforhodamine B was dissolved in Tris buffer I (50 mM Tris, 150 mM NaCl, pH=7.4 or 50 mM Tris, 150 mM NaCl, pH=4.5) at a concentration of 20 mM and pH was further adjusted to 7.4 or 4.5 by adding NaOH or HCl. Two milliliters of this solution were added to the dried lipid film and let hydrate for 30 minutes at ambient temperature. Afterwards, LUVs were prepared as described above by extrusion. The osmolarity of Tris buffer I (with sulforhodamine B) was determined and Tris buffer II (pH=7.4 or pH=4.5) was made with a NaCl concentration that equalized the osmolarity of Tris buffer I (with sulforhodamine B) at pH=7.4 or pH=4.5, respectively.

Sephadex® G-50 fine (Sigma Aldrich) was hydrated with Tris buffer II (pH=7.4 or pH=4.5) for around 3 hours before transferred onto a column with a volume of 6 ml. The gel was concentrated by 2-3 cycles of refilling and centrifuging the column for 2 minutes at 2000 g. Afterwards, 500 µl LUV were slowly added on the top center of each column and the column was centrifuged for 2 minutes at 2000 g. The elute contained vesicles with 20 mM sulforhodamine B inside, while the outer sulforhodamine B remained stuck in the column. Rouser assay was further used to determine the concentration of phospholipids[2].

Phosphate buffer was prepared at the same osmolarity as Tris buffer I/II (pH=7.4 or pH=4.5) to dilute vesicles to a final concentration of 100 µM phospholipids. One milliliter of vesicle suspension was transferred to a quartz cuvette containing a magnetic stirring bar and fluorescence intensity was recorded with a Cary Eclipse fluorescence spectrophotometer (Agilent, FL0904M005) at 565 nm excitation and 586 nm emission. Five microliter of different stock solutions of PC(16:0/9:0<CHO@C9>) and PC(16:0/9:0<COOH@C9>) in ethanol were added to the LUV suspension at 2 minutes recording to keep a constant concentration of ethanol. 0.1 % Triton X-100 was added after 20 minutes incubation to obtain maximum leakage (**Figure 3A**). All experiments were performed at 20°C.

1.8 Membrane packing quantification

For the membrane order measurements, we used three different probes, including di-4-ANEPPDHQ, Laurdan and DPH.

di-4-ANEPPDHQ

The vesicles were diluted with PBS to 1 ml at 100 µM, then 1 ml of 500 nM di-4-ANEPPDHQ in PBS was added to stain the vesicles. The final concentration for vesicles and di-4-ANEPPDHQ were 50 µM and 250 nM, respectively. The incubation was conducted at room temperature for 5 minutes in the dark. Fluorescence intensity was measured with the CLARIOstar (BMG LABTECH) in 96-well plates (Nunc black). The excitation wavelength was 488 nm and an emission wavelength scan was performed from 520 nm to 740 nm.

Laurdan

The same conditions and concentrations were used to incubate LUV with Laurdan except incubation was conducted at room temperature for 20 minutes in the dark. Fluorescence measurements were also performed in

the same conditions except that the excitation wavelength was 360 nm and the emission wavelength scan ranged from 400 nm to 600 nm.

DPH

DPH stock solution was dissolved in tetrahydrofuran (THF) freshly before use. DPH probe was diluted to 4 μM in a 0.2 mM LUV suspension and incubated for 20 minutes at room temperature. Fluorescence anisotropy was further measured with a Cary Eclipse fluorescence spectrophotometer (Agilent, FL0904M005) with an excitation at 340 nm and emission at 430 nm, respectively. The excitation light was passed through a vertically aligned polarizer while emission fluorescence was obtained at a switching vertical and horizontal polarizer filter. The anisotropy (r) is calculated based the formula: $r = (I_{VV} - I_{VH}) / (I_{VV} + 2I_{VH})$, of which I_{VV} and I_{VH} indicate the vertical and horizontal emission fluorescence intensity, respectively[3].

1.9 DLS analysis

LUV sizes and distribution were analyzed by dynamic light scattering (DLS) with a Malvern Zetasizer Nano-ZS at an angle of 173° for backscattering detection. Specifically, the vesicles were diluted to 0.5 mM phospholipids with PBS (38.38 mM Na_2HPO_4 and 19.62 mM NaH_2PO_4, NaCl 334.8 mM, pH 7.4). One milliliter LUV suspension was transferred into cuvette. Before each measurement, approximately 1 minute was used to equilibrate the distribution of vesicles. All measurements were conducted at 25 °C.

1.10 Surface tension determination with pendant drop tensiometer

For PBS buffer with LUVs, all PC(16:0/18:1) LUVs incorporated with different fractions of PC(16:0/9:0<CHO@C9>) and PC(16:0/9:0<COOH@C9>) were made in 400 mM KCl solutions (pH at 7.4 and 4.5) and further diluted in neutral PBS (30. 38 mM Na_2HPO_4 and 19.62 mM NaH_2PO_4, NaCl 334.8 mM, pH 7.4) and acidic PBS (49.79 mM NaH_2PO_4 and 350 mM NaCl, H_3PO_4 was used to adjust the final pH at 4.5) to a final concentration of 0.5 mM phospholipids.

For measurements of surface tension in PBS buffer not containing LUVs, a series of stock solutions of oxidized lipids in ethanol were prepared and 5 μl of each stock solution was added to 500 μl of PBS buffers (pH at 7.4 and pH at 4.5). Triton X-100, a powerful surfactant, was used at 0.1 % final concentration as a positive control and 0.5 % of ethanol was used as negative control. Liquid drops were formed and dispensed with 1 ml syringe together with OKI TE needle 20 GA (METCAL). Measurements of surface tension were carried out using a pendant drop tensiometer (DataPhysics OCA) by fitting the droplet shape with the Young–Laplace equation[4]. All measurements were conducted at room temperature.

1.11 ^{31}P-NMR analysis

Stock lipids, including 20 mM of PC(16:0/18:1), 1 mg/ml PC(16:0/9:0<CHO@C9>) and PC(16:0/9:0<COOH@C9>) were prepared in chloroform. Lipid mixtures were made by adding different amounts of stock solutions to reach final concentrations of 0, 5, 12, 15, 20 and 30 mol% for each oxidized lipid. Another lipid mixture containing both oxidized lipids at a total concentration of 20 mol% (10 mol% of PC(16:0/9:0<CHO@C9>) and 10 mol% PC(16:0/9:0<COOH@C9>)) was made. The total amount of each sample

was around 10 µmol. All lipid mixtures were dried with nitrogen stream at room temperature and in desiccator vacuum for 60 minutes. Five hundred microliters of Milli-Q-H_2O and/or 500 µl of 20 mM ammonium bicarbonate solution was added to hydrate the formed lipid film in a water bath (around 40 °C) for 30 minutes (avoid vortexing). Afterwards, all samples were lyophilized overnight, and the lipid powder was resuspended by 40 µl of Tris buffer (50 mM Tris, 150 mM NaCl, pH at 7.4) and subjected to 3 cycles of freeze-thawing in dry ice suspended in ethanol and warm water (around 40 °C).

The hydrated lipid suspensions were packed into 3.2 mm ssNMR rotors, assisted by mild (1000 g max) centrifugation. Static ^{31}P ssNMR spectra were recorded at a magnetic field of 11.7 T (500 MHz ^{1}H frequency) and a sample temperature of 290 K. 1D ^{31}P spectra were recorded using a 60 µs Hahn echo and 50 kHz SPINAL64 proton decoupling[5]. Spectra were apodised with 50 Hz exponential line broadening and baseline corrected.

1.12 Zeta (ζ) potential determination

The procedure for LUV making is conducted as described above in 400 mM KCl. The formed LUVs were diluted to 500 µM in phosphate buffers at different pHs which were made by following the recipes in the **Table 1** below. After dilution, all the liposomes were equilibrated for around 2 hours before measurement. Then one milliliter of LUVs suspension was transferred into the DTS 10170 cuvette (avoid bubbles), and the ζ-potential was measured with Malvern Zetasizer Nano-ZS. All measurements were conducted at 25 °C.

Table 1 Recipe of phosphate buffers used for zeta (ζ) potential determination

pH value	Chemicals
8.5	2.386 mM Na_2HPO_4, 47.614 mM NaH_2PO_4, 128. 5795 mM NaCl
7.5	33.307 mM Na_2HPO_4,16.693 mM NaH_2PO_4, 150.039 mM NaCl
6.5	49.998 mM NaH_2PO_4, 0.002 mM H_3PO_4, 199.9979 mM NaCl
5.5	49.979 mM NaH_2PO_4, 0.021 mM H_3PO_4, 199.9792 mM NaCl
4.5	49.792 mM NaH_2PO_4, 0.208 mM H_3PO_4, 199.7924 mM NaCl
3.5	47.999 mM NaH_2PO_4, 2.001 mM H_3PO_4, 197.9991 mM NaCl

1.13 MD simulations

The MD simulations of bilayers containing pure PC(16:0/18:1) and binary mixtures of PC(16:0/18:1) with 50 % oxidized PC(16:0/18:1) (i.e., PC(16:0/9:0<CHO@C9>) and PC(16:0/9:0<COOH@C9>))) were performed. Each of the bilayers was composed of 512 lipid molecules. In the bilayer with pure PC(16:0/18:1) lipids, a number of lipids was replaced by oxidized ones such that each of the two leaflets contained the same number of oxidized lipids.. Details of the systems are shown in **Table 2** below.

Table 2 List of simulated systems showing the proportion of molecules

System	Total No. lipid	NO. PC16:0/18:1)	NO. OxPCs	NO. of total solvent molecules	NO. Na^+
PC(16:0/18:1)	512	512	0	25600	–
50 mol% CHO@C9	512	256	256	25600	–
50 mol% COOH@C9	512	256	256	25344	256

All the calculations were performed using the Groningen Machine for Chemical Simulation (GROMACS)[6]. The parameters for all simulations were compatible with the united atom Gromos54a7 force field[7]. The atomic coordinates and united atom parameters of the PC(16:0/18:1) lipids were taken from Poger and Mark[8], and for PC(16:0/9:0<COOH@C9>) and PC(16:0/9:0<CHO@C9>) lipids parameters were determined using the Automated Topology Builder[9]. After energy minimization using the steepest descents algorithm, the MD simulations of bilayers containing pure PC(16:0/18:1) lipids and bilayers containing oxidized PC(16:0/18:1) lipids were run for 1 μs and 2 μs, respectively, with a time step of 2 fs.

All simulations were performed in the constant particle number-constant pressure-constant temperature (NPT) ensemble. The temperature was set to 300 K by the velocity-rescale algorithm applied separately to the lipids and water (ions were grouped with water) with a time constant of 0.1 ps[10]. The pressure was kept constant at 1 bar by applying a semi-isotropic pressure using the Parrinello-Rahman algorithm with a time constant of 3 ps and compressibility of 4.5×10^{-5} bar^{-1}[11]. Periodic boundary conditions were applied in all dimensions. All bond lengths were constrained using the P-LINCS algorithm[12]. A cutoff of 1.0 nm was used for Lennard-Jones and the real space part of the electrostatic interactions. The particle-mesh Ewald (PME) method was used to compute the long-range part of the electrostatic interactions with a 0.12 nm grid in the reciprocal-space and cubic interpolation of 4[13,14]. Water molecules were modeled using the simple point-charge (SPC) model[15]. Sodium counterions (Na^+) were added to the systems containing PC(16:0/9:0<COOH@C9>) to retain overall charge neutrality. Visual Molecular Dynamic (VMD) software was used to visualize membrane structures[16].

1.14 MD Trajectory Analysis

Atomistic MD simulations simulated at least 1 μs, and the last 500 ns were used for data analyses. The area per lipid (APL) was calculated by the area in the x-y plane (A) of the simulation box divided by the number of lipids in one leaflet. Bilayer thickness (h) was determined based on the positions of the phosphorus (P) atoms in the lipid headgroups. We calculated the area compressibility modulus (K_A) and the bending modulus (K_c) from the area and thickness fluctuations

$\boldsymbol{K_A = \frac{Ak_BT}{{\sigma_A}^2}}$, and $\boldsymbol{K_c = \frac{K_A(h-h_o)^2}{24}}$, respectively[17].

$\boldsymbol{\sigma_A}$ is the variance of the area box, $\boldsymbol{k_B}$ is Boltzmann constant, **T** is temperature and $\mathbf{h_o}$ is equal to 1 nm due to the assumption for pure POPC bilayers in the liquid phase.

Permeability (P) of water molecules through the membrane bilayer was studied by Fick's first law[18],

$$\mathbf{P = \frac{(dn/dt)}{A \cdot \Delta c}},$$

where dn/dt is the rate of the number of water molecules passing through the membrane, $\Delta C=C_{waterbulk}-C_{hydrophobiccore}$ is the water concentration gradient (the number of water molecules per nm^3) and the water concentration in the hydrophobic core is negligible $C_{hydrophobiccore}=0$).

2. Additional Figures

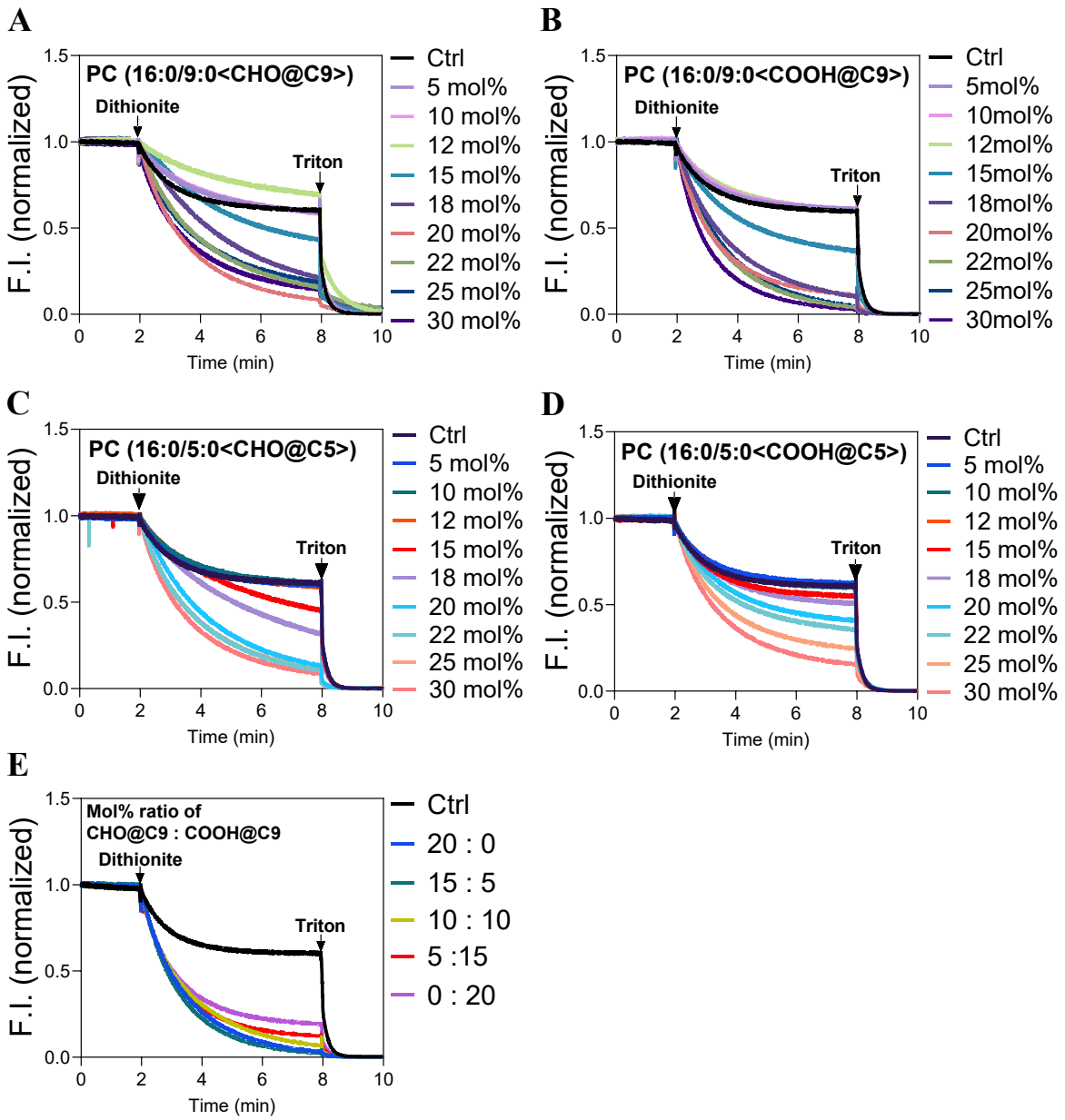

Figure S1. Incorporation of OxPCs disrupts membrane in PC(16:0/18:1) LUVs. Kinetics of NBD-PE(18:1/18:1) fluorescence quenching in LUVs incorporated with different fractions of (**A**) PC(16:0/9:0<CHO@C9>) and (**B**) PC(16:0/9:0<COOH@C9>), (**C**) PC(16:0/5:0<CHO@C5>) and (**D**) PC(16:0/5:0<COOH@C5>). (**E**) Time dependent of NBD-PE(18:1/18:1) fluorescence quenching in LUVs incorporated by varied ratios of PC(16:0/9:0<CHO@C9>) and PC(16:0/9:0<COOH@C9>) at a total fraction of 20 mol%.

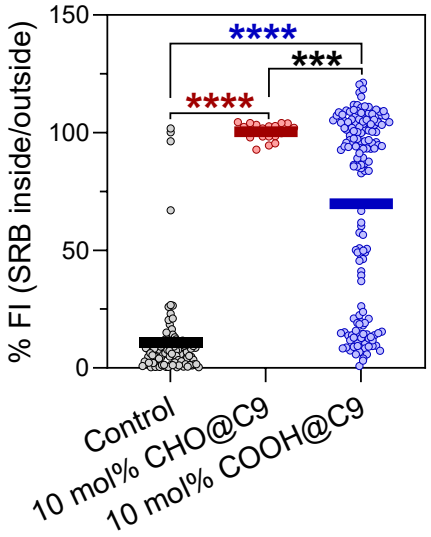

Figure S2. Sulforhodamine (SRB) leakage in PC(16:0/18:1) GUVs incorporated with 10 mol% of PC(16:0/9:0<CHO@C9>) and PC(16:0/9:0<COOH@C9>) at pH 7.4. The bar corresponds to average leakage. One-way ANOVA analysis was used to compare the differences between groups (***p<0.001, ****p<0.0001).

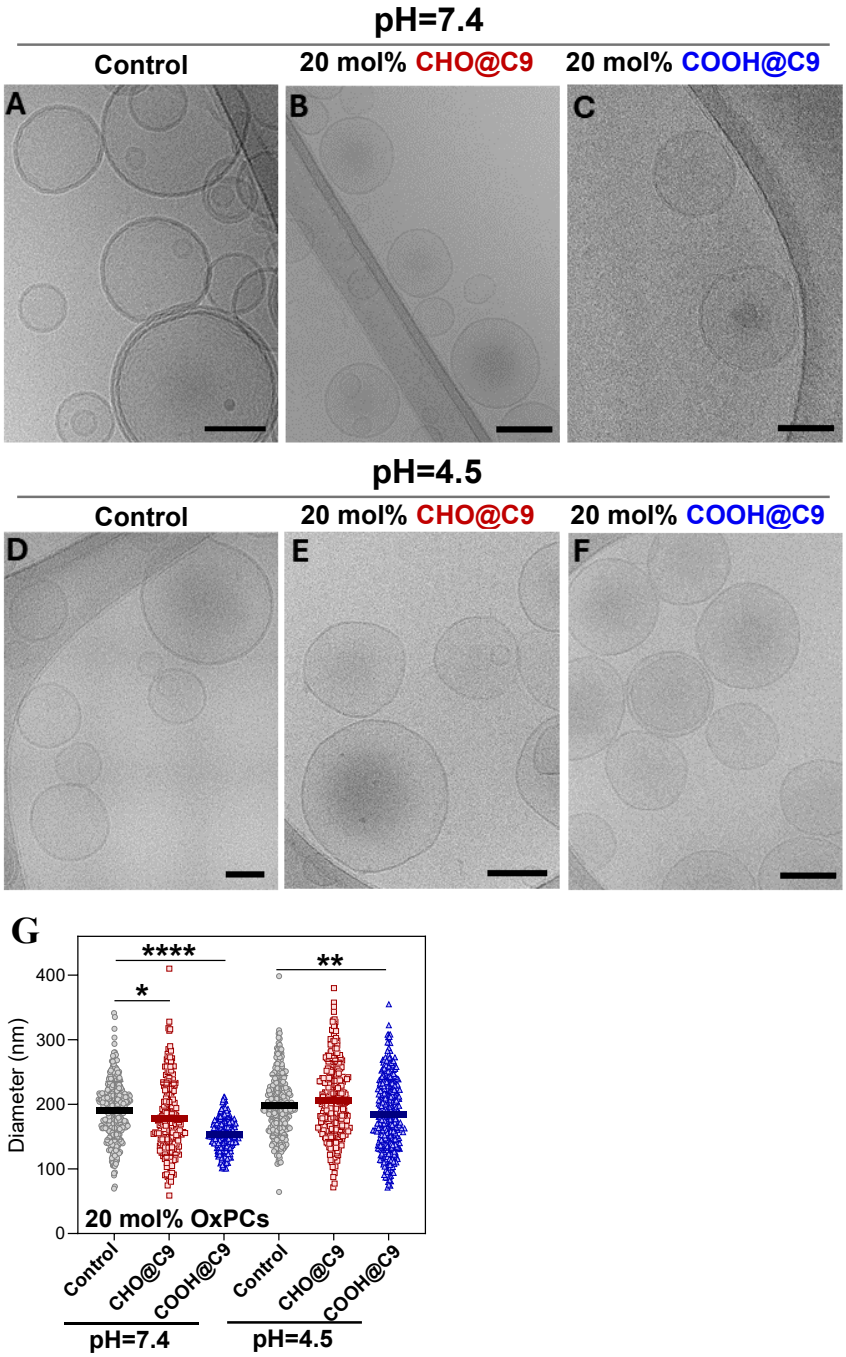

Figure S3. Cryo-electron microscopy (Cryo-EM) images of PC(16:0/18:1) LUVs incorporated with OxPC's at pH 7.4 (A, B, C) and pH 4.5 (D, E, F). PC(16:0/18:1) control in PBS (**A, D**) . PC(16:0/18:1) LUVs incorporated with 20 mol% PC(16:0/9:0<CHO@C9>) (**B, E**) and 20 mol% PC(16:0/9:0<COOH@C9>) (**C**, **F**) The scale bar is 100 nm. (**G**) Quantification of diameter size in LUV samples imaged by Cryo-EM. One-way ANOVA analysis was used to compare the differences between conditions, *p<0.05, **p<0.01, ****p<0.0001. Multi-lamellarity was at a similar percentage of approximately 4 % in all samples.

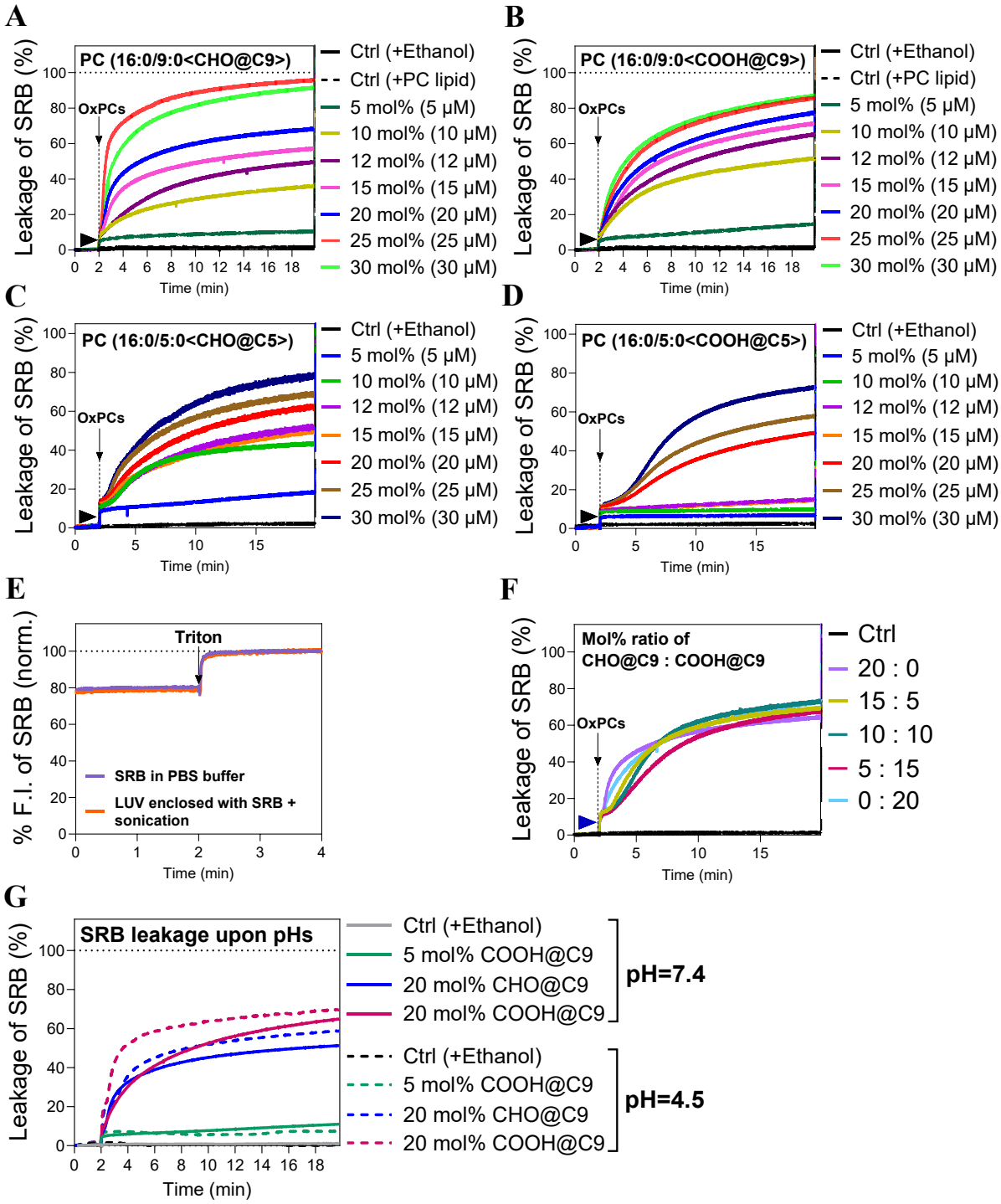

Figure S4. Permeabilization of PC(16:0/18:1) LUV induced by addition of OxPCs. Sulforhodamine B leakage from LUVs after addition (arrows) of different concentrations of (**A**) PC(16:0/9:0<CHO@C9>), (**B**) PC(16:0/9:0<COOH@C9>), (**C**) PC(16:0/5:0<CHO@C5>) and (**D**) PC(16:0/5:0<COOH@C5>), respectively. The addition of PC(16:0/18:1), ethanol was used as control. (**E**) Increase of fluorescence when Triton-X 100 was added to either sulforhodamine B in PBS or PC(16:0/18:1) LUVs enclosed with 20 mM sulforhodamine B inside of lumen. (**F**) Permeabilization of PC(16:0/18:1) LUVs induced by various ratios of PC(16:0/9:0<CHO@C9>) and PC(16:0/9:0<COOH@C9>) at a total fraction of 20 mol%. (**G**) Sulforhodamine B leakage from LUVs at pH 7.4 (solid line) or 4.5 (dashed line) after addition (arrows) of PC(16:0/9:0<CHO@C9>) or PC(16:0/9:0<COOH@C9>).

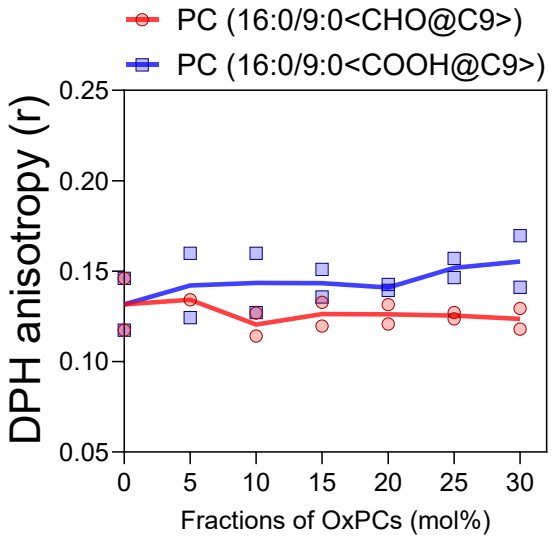

Figure S5. DPH (1,6-diphenyl-1,3,5-hexatriene) anisotropy upon increasing fractions of PC(16:0/9:0<CHO@C9>) and PC(16:0/9:0<COOH@C9>) integrated into PC(16:0/18:1) LUV. Two independent experiments have been done in triplicates (n≥2).

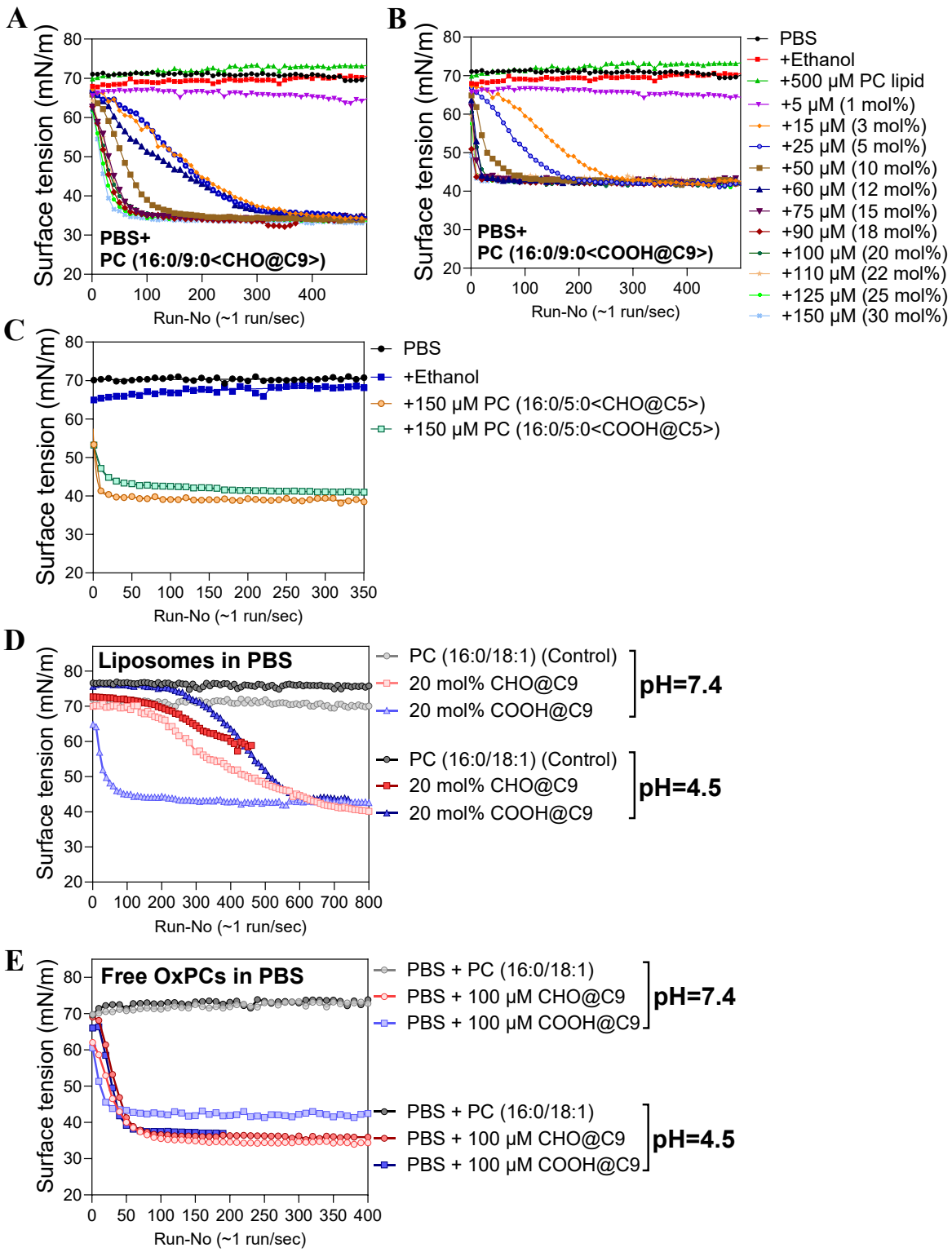

Figure S6. Surface tension determination with pendant drop tensiometry. Interfacial tension of PBS at pH 7.4 in presence of (**A**) PC(16:0/9:0<CHO@C9>), (**B**) PC(16:0/9:0<COOH@C9>), and (**C**) PC(16:0/5:0<CHO@C5>) and PC(16:0/5:0<COOH@C5>). (**D**) Comparison of surface tension of PBS suspensions at pH 7.4 and 4.5 containing PC(16:0/18:1) LUVs that have been incorporated with 20 mol% PC(16:0/9:0<CHO@C9>) and PC(16:0/9:0<COOH@C9>) upon inspection time. (**E**) Comparison of surface tension of PBS at pH 7.4 and 4.5 after the addition of PC(16:0/9:0<CHO@C9>) and PC(16:0/9:0<COOH@C9>) to the buffer. One percent of ethanol in PBS was used as negative control. At least three independent experiments were performed (n≥3).

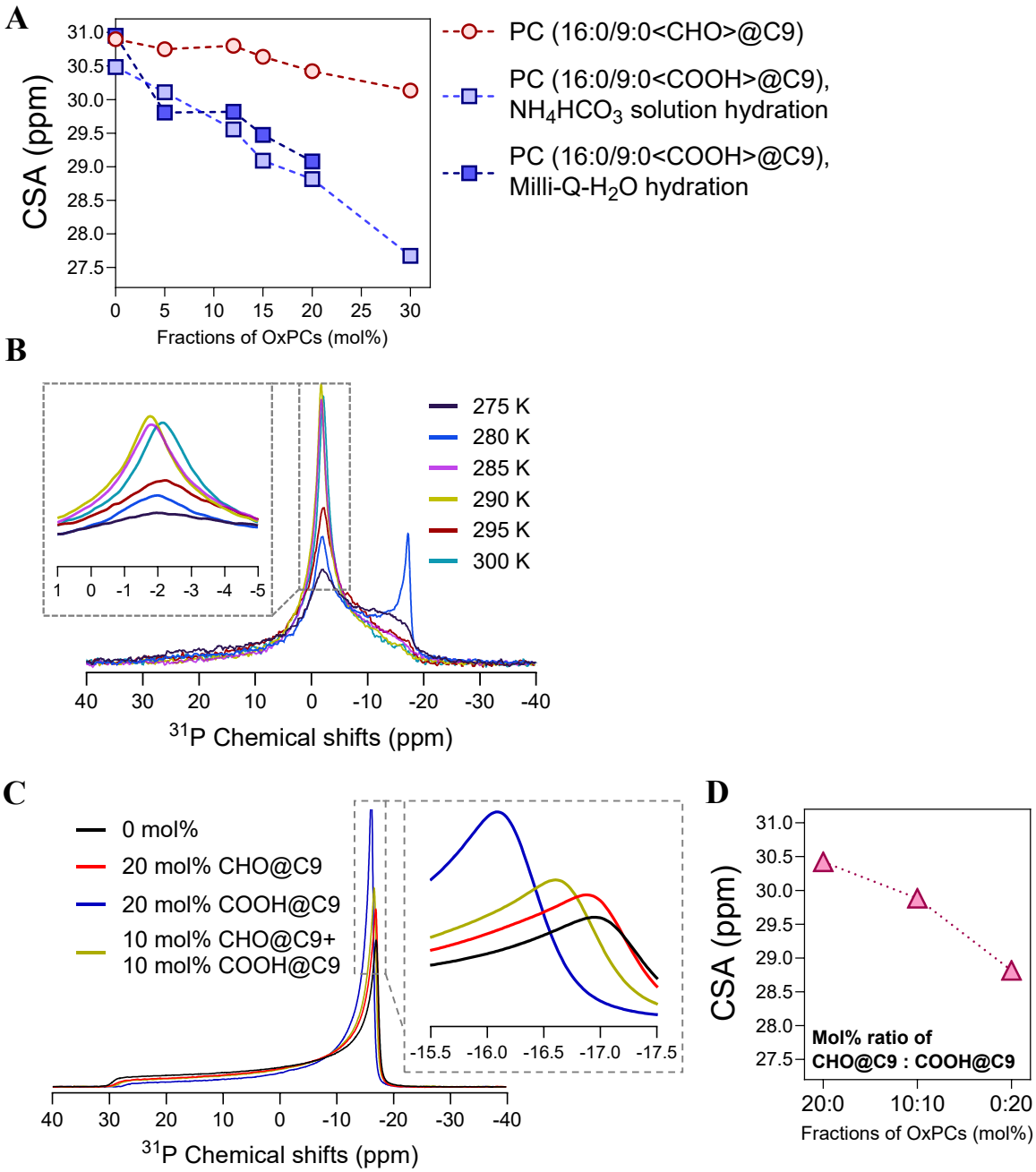

Figure S7. ^{31}P-NMR analysis. (**A**) Chemical shift anisotropy (CSA, Δ/ppm) of PC(16:0/18:1) MLVs incorporated with different fractions of PC(16:0/9:0<CHO@C9>) or PC(16:0/9:0<COOH@C9>). (**B**) Static ^{31}P NMR spectra of PC(16:0/18:1) MLVs with 5 mol% PC(16:0/9:0<COOH@C9>) and neutralized by NaOH upon temperature gradients. Static ^{31}P NMR spectra of PC(16:0/18:1) MLVs with (**C**) varied ratios between PC(16:0/9:0<CHO@C9>) and PC(16:0/ 9:0<COOH@C9>) at a total fraction of 20 mol%. (**D**) Chemical shift anisotropy (CSA, Δ/ppm) of PC(16:0/18:1) MLVs incorporated with varying ratios of PC(16:0/9:0<CHO@C9>) and PC(16:0/ 9:0<COOH@C9>) at a total fraction of 20 mol% in MilliQ-H_2O.

3. References

(1) Weinberger, A.; Tsai, F. C.; Koenderink, G. H.; Schmidt, T. F.; Itri, R.; Meier, W.; Schmatko, T.; Schröder, A.; Marques, C. Gel-Assisted Formation of Giant Unilamellar Vesicles. *Biophys J* **2013**, *105* (1), 154–164. https://doi.org/10.1016/j.bpj.2013.05.024.

(2) Rouser, G.; Kritchevsky, G.; Galli, C.; Heller, D. Determination of Polar Lipids: Quantitative Column and Thin-Layer Chromatography. *J Am Oil Chem Soc* **1965**, *42* (3), 215–227. https://doi.org/10.1007/BF02541135.

(3) Sousa, T.; Castro, R. E.; Coutinho, A.; Rodrigues, C. M. P.; Prieto, M.; Fernandes, F. Measuring the Impact of Bile Acids on the Membrane Order of Primary Hepatocytes and Isolated Mitochondria by Fluorescence Imaging and Spectroscopy BT - Experimental Cholestasis Research; Vinken, M., Ed.; Springer New York: New York, NY, 2019; pp 99–115. https://doi.org/10.1007/978-1-4939-9420-5_7.

(4) Berry, J. D.; Neeson, M. J.; Dagastine, R. R.; Chan, D. Y. C.; Tabor, R. F. Measurement of Surface and Interfacial Tension Using Pendant Drop Tensiometry. *J Colloid Interface Sci* **2015**, *454*, 226–237. https://doi.org/https://doi.org/10.1016/j.jcis.2015.05.012.

(5) Rance~, M.; Byrd, R. A. *Obtaining High-Fidelity Spin-l/2 Powder Spectra in Anisotropic Media: Phase-Cycled Hahn Echo Spectroscopy**; 1983; Vol. 52.

(6) Abraham, M. J.; Murtola, T.; Schulz, R.; Páll, S.; Smith, J. C.; Hess, B.; Lindah, E. Gromacs: High Performance Molecular Simulations through Multi-Level Parallelism from Laptops to Supercomputers. *SoftwareX* **2015**, *1–2*, 19–25. https://doi.org/10.1016/j.softx.2015.06.001.

(7) Schmid, N.; Eichenberger, A. P.; Choutko, A.; Riniker, S.; Winger, M.; Mark, A. E.; Van Gunsteren, W. F. Definition and Testing of the GROMOS Force-Field Versions 54A7 and 54B7. *European Biophysics Journal* **2011**, *40* (7), 843–856. https://doi.org/10.1007/s00249-011-0700-9.

(8) Poger, D.; Mark, A. E. On the Validation of Molecular Dynamics Simulations of Saturated and Cis-Monounsaturated Phosphatidylcholine Lipid Bilayers: A Comparison with Experiment. *J Chem Theory Comput* **2010**, *6* (1), 325-336. https://doi.org/10.1021/ct900487a.

(9) Malde, A. K.; Zuo, L.; Breeze, M.; Stroet, M.; Poger, D.; Nair, P. C.; Oostenbrink, C.; Mark, A. E. An Automated Force Field Topology Builder (ATB) and Repository: Version 1.0. *J Chem Theory Comput* **2011**, *7* (12), 4026–4037. https://doi.org/10.1021/ct200196m.

(10) Bussi, G.; Donadio, D.; Parrinello, M. Canonical Sampling through Velocity Rescaling. *J Chem Phys* **2007**, *126* (1), 014101. https://doi.org/10.1063/1.2408420.

(11) Parrinello, M.; Rahman, A. Polymorphic Transitions in Single Crystals: A New Molecular Dynamics Method. *J Appl Phys* **1981**, *52* (12), 7182–7190. https://doi.org/10.1063/1.328693.

(12) Hess, B. P-LINCS: A Parallel Linear Constraint Solver for Molecular Simulation. *J Chem Theory Comput* **2008**, *4* (1), 116–122. https://doi.org/10.1021/ct700200b.

(13) Darden, T.; York, D.; Pedersen, L. Particle Mesh Ewald: An N·log(N) Method for Ewald Sums in Large Systems. *J Chem Phys* **1993**, *98* (12), 10089–10092. https://doi.org/10.1063/1.464397.

(14) Essmann, U.; Perera, L.; Berkowitz, M. L.; Darden, T.; Lee, H.; Pedersen, L. G. A Smooth Particle Mesh Ewald Method. *J Chem Phys* **1995**, *103* (19), 8577–8593. https://doi.org/10.1063/1.470117.

(15) Berendsen, H. J. C.; Postma, J. P. M.; van Gunsteren, W. F.; Hermans, J. Interaction Models for Water in Relation to Protein In: Pullman, B. (eds) Intermolecular Forces. The Jerusalem Symposia on Quantum Chemistry and Biochemistry, vol 14. Springer, Dordrecht. https://doi.org/10.1007/978-94-015-7658-1_21.

(16) Humphrey, W.; Dalke, A.; Schulten, K. *VMD: Visual Molecular Dynamics*; 1996 Feb 1;14(1):33-8. https://doi.org/10.1016/0263-7855(96)00018-5.

(17) Waheed, Q.; Edholm, O. Undulation Contributions to the Area Compressibility in Lipid Bilayer Simulations. *Biophys J* **2009**, *97* (10), 2754-2760. https://doi.org/10.1016/j.bpj.2009.08.048.

(18) Bhatia, T.; Robinson, T.; Dimova, R. Membrane Permeability to Water Measured by Microfluidic Trapping of Giant Vesicles. *Soft Matter* **2020**, *16* (31), 7359-7369. https://doi.org/10.1039/d0sm00155d.